AIMS Geosciences

AIMS Geosciences, 7(3): 355–389.
DOI: 10.3934/geosci.2021022
Received: 07 July 2021
Accepted: 19 August 2021
Published: 23 August 2021

http://www.aimspress.com/journal/geosciences

Research article

Very low-grade metamorphism of the Dezadeash Formation (Jura-Cretaceous): Constraints on the tectonometamorphic history of the Dezadeash flysch basin and implications regarding the tectonic evolution of the Northern Cordillera of Alaska and Yukon

Grant W Lowey*

Whitehorse, Yukon. Canada

* **Correspondence:** Email: loweygrant@gmail.com; Tel: (867)633–6828.

Abstract: Mesozoic convergence of the Wrangellia composite terrane with the western margin of North America resulted in the collapse of intervening flysch basins. One of these basins, the Jurassic-Cretaceous Gravina-Nuzotin belt, comprises from south to north, the Gravina sequence and Gravina belt in southeastern Alaska, the Dezadeash Formation in Yukon, and the Nutzotin Mountains sequence in eastern Alaska. Previous work shows that the Gravina sequence and Gravina belt were underthrust >20 km beneath the margin of North America in mid-Cretaceous time, culminating in amphibolite facies metamorphism. This tectonometamorphic scenario was subsequently applied to the entire Gravina-Nutzotin belt, despite any detailed studies pertaining to the tectonometamorphic evolution of the Dezadeash Formation. The present analysis of the Dezadeash Formation reveals that metamorphic mineral assemblages in sandstone and tuff document subgreenschist, high temperature zeolite facies metamorphism; Kübler indices of illite and Árkai indices of chlorite in mudstone record diagenetic to high anchizone metapelitic conditions; and the color of organic matter (i.e., the Thermal Alteration Index of palynomorphs and the Conodont Alteration Index) and pyrolysis of organic matter in mudstone and hemipelagite beds document thermal maturation at catagenesis to mesogenesis stages. Collectively, the mineralogic and organic thermal indicators in the Dezadeash Formation suggest that strata experienced maximum pressure-temperature conditions of 2.5 ± 0.5 kbar and 250 ± 25 °C in the Early Cretaceous. The inferred tectonometamorphic evolution of the Dezadeash Formation does not support the northern part of the Gravina-Nutzotin belt being underthrust >20 km beneath

the western margin of North America in mid-Cretaceous time, thus contrasting sharply with the Gravina sequence and Gravina belt in the southern part of the Gravina-Nutzotin belt. The diverse tectonometamorphic histories recorded by the southern and northern parts of the Gravina-Nutzotin belt may be a manifestation of oblique collision and diachronous south-to-north accretion of the Wrangellia composite terrane to North America.

Keywords: tectonic setting; flysch basin; North American cordillera; Gravina-Nutzotin belt; Dezadeash Formation; subgreenschist facies

1. Introduction

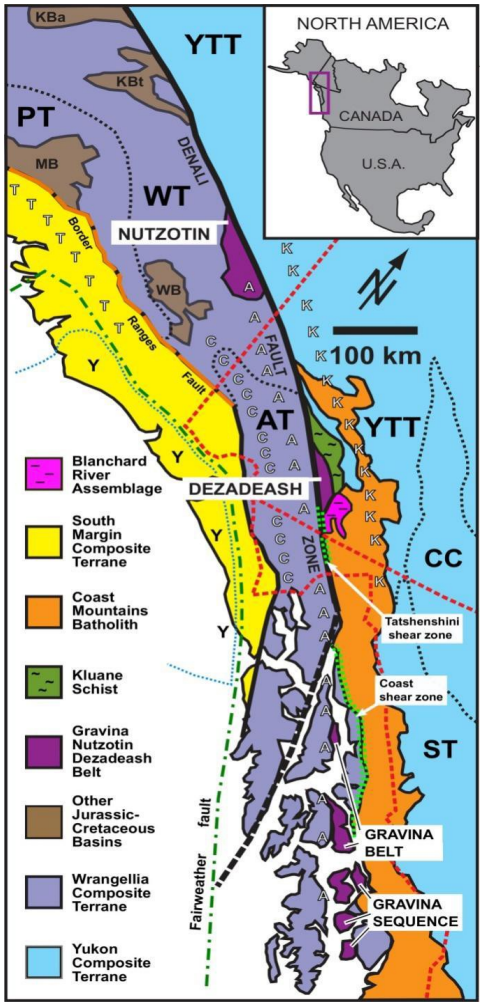

Figure. 1. Location map and geologic setting of the Dezadeash Formation, Yukon [1–3]. AT, Alexander terrane; CC, Cache Creek terrane; PT, Peninsular terrane; ST, Stikine terrane; Y, Yakutat terrane; YTT, Yukon-Tanana terrane; WT, Wrangellia terrane. Kootenay, Cassiar, and Quesnel terranes not shown. Other Jurassic-Cretaceous basins not part of the Gravina-Nutzotin belt: KBa, Kahiltna basin-Alaska Range; KBt, Kahiltna basin-Talkeetna Mountains; MB, Matanuska Valley basin; WB, Wrangell Mountains basin; T, Talkeetna arc; C, Chitina arc; A, Chisana arc; K, Kluane arc.

The Mesozoic convergence and subsequent collision of the Wrangellia composite terrane (WCT) against the western margin of North America, represented by the Yukon composite terrane (YCT), was accompanied by the collapse of several intervening flysch basins. The flysch basins are preserved as relatively thick, variably deformed Jurassic-Cretaceous sedimentary and volcanic rocks scattered along the Northern Cordillera of Alaska and Yukon (Figure 1). One of the best studied flysch basins is the Gravina-Nutzotin belt [4], comprising, from south to north, the Gravina sequence and Gravina belt in southeastern Alaska (herein referred to as the "southern" part of the Gravina-Nutzotin belt), and the Dezadeash Formation in Yukon and the Nutzotin Mountains sequence in east-central Alaska (herein referred to as the "northern" part of the Gravina-Nutzotin belt) (Figure 1).

Previous work on the southern part of the Gravina-Nutzotin belt (i.e., the Gravina sequence and Gravina belt in southeastern Alaska) demonstrated that these rocks were tectonically emplaced beneath the YCT along a regionally extensive (1200 km long) west-vergent thrust system in the mid-Cretaceous [5–8]. A regional magnetotelluric survey in east-central Alaska identified a very-low resistivity layer beneath YCT rocks extending from about 10 km to 20 km in depth, which was interpreted as tectonically underthrust Mesozoic flysch [9]. This interpretation was apparently supported by a refraction/wide-angle reflection seismic survey that suggested the presence of reflective and near-horizontal layering beneath YCT rocks from approximately 8 to 27 km depth [10]. Subsequently, the mid-Cretaceous thrust system was implicated in the metamorphism and deformation of the entire Gravina-Nutzotin belt [11].

However, additional studies cast doubt on the existence of underthrust Mesozoic flysch [12–14]. The very-low resistivity layer identified previously was likely highly conductive YCT rocks and not underthrust flysch [12]; the very-low resistivity layer was suggested to be the result of lower-crustal fluids in YCT rocks [13]; and isotopic evidence was presented discounting the magnetotelluric, Mesozoic underthrust flysch interpretation [14]. Nevertheless, researchers continue to invoke the underthrust flysch scenario for interpreting the structural deformation and crustal-scale structure of the Northern Cordillera [15–19], despite any detailed studies of the tectonometamorphic history of the northern part of the Gravina-Nutzotin belt.

The purpose of this paper is to characterize the metamorphic character of the Dezadeash Formation, including the metamorphic grade, maximum temperature and pressure reached by the strata, timing of metamorphism, and type of metamorphism. The study presents the results of a multidisciplinary analysis of the Dezadeash Formation, comprising: structural fabrics observed in outcrop; petrographic examination of thin sections of sandstones, mudstone, hemipelagite, and volcaniclastic beds; X-ray diffraction of sandstone, mudstone, hemipelagite, and volcaniclastic beds, including whole-rock, clay speciation, and illite Kübler index and chlorite Árkai index "crystallinity" determinations; microfossil analysis of mudstone and hemipelagite beds for palynomorphs and limestone clasts for conodonts; and programmed pyrolysis maturation analysis of mudstones and hemipelagites. Published thermochronometric data from the Dezadeash Formation are also incorporated. The aim of the paper is to constrain the tectonometamorphic evolution of the Dezadeash Formation, which has implications regarding the convergence and subsequent accretion of the WCT to the Mesozoic margin of North American, particularly with regards to the mid-Cretaceous west-vergent thrust system in the Northern Cordillera.

2. Geologic setting

The Northern Cordillera of North America is an amalgamation of allochthonous composite terranes, superimposed magmatic arcs, and exhumed sedimentary flysch basins, all variably offset by lithospheric-scale strike-slip faults. Geologic elements relevant to this study include (Figure 1): the Yukon and Wrangellia composite terranes; the Chitina, Chisana, and Kluane arcs; the Gravina-Nutzotin belt flysch basins (i.e., the Dezadeash Formation, Nutzotin Mountains sequence, Gravina sequence, and Gravina belt); the Blanchard River assemblage and Kluane Schist high-grade metamorphic belts; and the Denali fault and Coast-Tatshenshini shear zone.

2.1. Yukon and Wrangellia composite terranes

The Yukon composite terrane (YCT) consists of the polymetamorphosed and polydeformed, pericratonic and arc-related Yukon-Tanana, Slide Mountain, Cache Creek, Quesnellia, and Stikinia terranes (Figure 1) [1–3]. The YTC was accreted to North America during the mid-Jurassic [2,20], thus forming the Mesozoic margin of North America.

The Wrangellia composite terrane (WCT) is an amalgamation of three tectonostratigraphic terranes referred to as the Alexander, Wrangellia, and Peninsular terranes (Figure 1) [21]. These represent Neoproterozoic to Mesozoic island arc-related volcanic and sedimentary rocks [23,24]. The WCT is interpreted as part of an obliquely converging oceanic plateau [25] that was emplaced against the Mesozoic margin of North America along a regionally extensive, mid-Cretaceous, west-vergent thrust system [7,11,22,26]. Although there is general agreement that convergence and accretion were diachronous—including closure of the intervening flysch basins—there are conflicting interpretations whether accretion propagated zipper-like south-to-north or north-to-south [16,27–33].

2.2. Chitina, Chisana, and Kluane magmatic arcs

The Late Jurassic-Early Cretaceous Chitina arc (~160–140 Ma) ("C" in Figure 1) is restricted to the Wrangell and Alexander terranes along the outboard margin of the WCT [22,34–36]. Extensive volcanic and volcaniclastic rocks derived from the Chitina arc are scattered throughout the Gravina-Nutzotin belt: generally volcanic and volcaniclastic rocks occur in the southern part of the belt (i.e., Gravina belt and Gravina sequence), and only volcaniclastic rocks occur in the northern part of the belt (i.e., Dezadeash Formation and Nutzotin Mountains sequence) [22]. Plutonic rocks interpreted as the roots of the Chitina arc extend throughout the Northern Cordillera. The plutonic rocks occur as elongate batholithic complexes consisting mainly of quartz diorite, tonalite and granodiorite that range from Late Jurassic to Early Cretaceous in age (~160–130 Ma) [34,35,37].

The Late Cretaceous Chisana arc (~120–105 Ma) ("A" in Figure 1) is restricted to the Wrangell and Alexander terranes along the inboard margin of the WCT [16,38]. Extensive volcanic and volcaniclastic rocks derived from the Chisana arc are scattered throughout the Gravina-Nutzotin belt (i.e., Gravina belt and Gravina sequence, and Nutzotin Mountains sequence). In addition, plutonic rocks interpreted as the roots of the Chisana arc also extend throughout the Northern Cordillera. The plutonic rocks occur as elongate batholithic complexes and plutons consisting of granodiorite, quartz diorite, diorite, and rarer quartz monzonite that are Early Cretaceous in age (~117–106 Ma) [34,35,37].

One of these plutonic complexes, referred to as the Shorty Creek pluton, intrudes the Dezadeash Formation in southwest Yukon (Figure 2), and has a K-Ar age of ~106 Ma [37]. Roots of the Chisana arc are also preserved as Alaskan-type ultramafic complexes: the Pyroxenite Creek ultramafic complex in southwestern Yukon (Figure 2) intrudes the Dezadeash Formation and has K-Ar ages of ~128–109 Ma and a Rb-Sr age of ~116 Ma (Rb-Sr) [39].

The Late Cretaceous-Paleogene Kluane arc (~85–45 Ma) ("K" in Figure 1) occurs much farther inboard than either the Chitina and Chisana arcs [40–41]. Plutonic rocks interpreted as the roots of the Kluane arc form part of the extensive Coast Plutonic Complex or Coast Mountains Batholith (~175–45 Ma) that extends for much of the length of the Northern Cordillera (Figure 1) [42,43]. The plutonic rocks occur as batholithic complexes consisting mainly of diorite, quartz diorite, granodiorite and locally monzonite, and syenite [34]. The Coast Plutonic Complex intrudes both the WCT and the YCT is inferred to have formed immediately after accretion of the WCT with the YCT (i.e., the ancient margin of western North America), thereby obscuring the "Shakwak" suture between these two composite terranes [41,44].

2.3. Gravina-Nutzotin belt flysch basins

The Dezadeash Formation is an approximately 3000 m thick succession of thin- to thick-bedded turbidites and massive sandstone with minor amounts of conglomeratic mudstone containing limestone clasts up to ~10 m in exposed longest dimensions, volcaniclastic rocks, and hemipelagic lime mudstone [45–47]. Based on detailed lithofacies analysis, the Dezadeash Formation represents mainly the middle and lower subdivisions of a point-source, mud/sand-rich submarine fan that was derived from the WCT and Chitina arc [47,48].

The Dezadeash Formation is Late Jurassic (Oxfordian) to Early Cretaceous (Valanginian) in age based on collections of the bivalve *Buchia* [45], and uncomfortably overlies the Alexander and Wrangellia terranes [49]. The Dezadeash Formation is overlain unconformably by ~1000 m of unmetamorphosed nonmarine Paleogene clastic and volcaniclastic rocks of the Amphitheater Formation [45,50].

Two phases of folding have been identified in the Dezadeash Formation: the oldest folds (F_1) trend northerly, are asymmetric or overturned to the east, and locally change laterally into thrust faults; the youngest folds (F_2) trend west-northwesterly and are open [45]. The oldest folds are crosscut by the Shorty Creek pluton that reveals a K-Ar age of ~106 Ma [37] and they are attributed to movement on a—"tectonic slope" because the trend of the folds is similar to the trend of penecontemporaneous slump folds in the Dezadeash Formation [45]. The youngest folds (F_2) are ascribed to westward directed thrusting of the Kluane Schist over the Dezadeash Formation and movement on the Denali fault zone. Both the Kluane Schist and Denali fault are described later [45].

The Dezadeash Formation has also been utilized in low-temperature thermochronometric investigations. Specifically, two samples from the St. Elias Mountains syntaxis in southwest Yukon (Figure 2) [51] are summarized in Table 1. The thermochronometric investigations reveal multiple episodes of exhumation and landscape evolution attributed to rapid cooling at ~95–75 Ma due to accretion of the WCT to the YCT, slow cooling during ~75–30 Ma caused by relief degradation, and renewed rapid cooling beginning ~30 Ma and continuing to the present, attributed to flat-slab subduction of the Yakutat terrane and strike-slip displacement on the Denali fault zone [54].

Table 1. Published low-temperature thermochronometric data, Dezadeash Formation, Yukon, Canada.

Sample	Lithology	Elevation (m)	AHe (Ma)	ZHe (Ma)	AFT (Ma)	ZFT (Ma)
KLB04	metapelite	605	17.8 ±1.6	59.7 ±8.1	n.a.	n.a.
KLB91	mudstone	725	11.4 ±0.8	68.8 ±2.3	n.a.	109.9 ±8.9
T_c (ºC)			70	180	120	240
PRZ (ºC)			40–70	130–180	n.a.	n.a.
PAZ (ºC)			n.a.	n.a.	60–120	180–240

Note: Samples KLB04 and KLB91 from [51]. •AHe = apatite (U-Th)/He, ZHe = zircon (U-Th)/He, AFT = apatite fission-track, and ZFT = zircon fission-track thermochronometer age; •T_c = closure temperature (radioactive decay product retained below this temperature, but not above it; also referred to as the temperature of a mineral at the time given by its radiometric age); •PRZ = partial retention zone (temperature window over which radioactive decay product is retained); •PAZ = partial annealing zone (temperature window over which radioactive decay product is preserved). Closure temperatures from [52,53]. Note that the temperatures are only approximate because they depend on the cooling rate, chemistry of the mineral, and grain-size of the mineral [52].

The Nutzotin Mountains sequence is the proximal half of the Nutzotin-Dezadeash basin that was offset by the Denali fault (described later). The Nutzotin Mountains sequence is up to 3000 m thick and consists mainly of thin-bedded turbidites with minor amounts of massive sandstone, conglomeratic mudstone containing limestone clasts up to ~10 m exposed longest dimensions, as well as hemipelagite beds [4,55–57]. The strata are interpreted as westerly sourced, distal to proximal submarine fan deposits that grade upward into shelf deposits [56,57]. The Nutzotin Mountains sequence is Late Jurassic (Tithonian) to Early Cretaceous (Valanginian) in age and unconformably overlies the Wrangellia terrane [58]. The strata are unmetamorphosed and deformed by north-dipping thrust faults and overturned folds that are crosscut by 117–105 Ma plutons [57].

The Gravina sequence consists ~2200 m of mainly metavolcanic rocks and minor amounts of metasedimentary rocks [59]. U-Pb zircon ages (154–158 Ma) of granitic clasts and rare fossils suggest a Late Jurassic in age [59]). The sequence is interpreted as submarine lava flows and submarine fans deposited on the flanks a volcanic arc [59]. The Gravina sequence experienced greenschist to amphibolite facies metamorphism related to the mid-Cretaceous, regionally extensive west-vergent thrust system [7,8].

The Gravina belt includes a lower, ~1000 m thick unit of mafic volcanic and volcaniclastic rocks inferred to be Late Jurassic in age [60,61], and an upper, ~1800 m thick sequence of sandstone and mudstone turbidites with minor amounts of conglomerate referred to as the Seymour Canal Formation [60,62]. Fossils indicate the Seymour Canal Formation is Late Jurassic to Early Cretaceous, and strata are interpreted as upper and middle submarine fan deposits sourced from the WCT [62]. The Gravina belt was subject to zeolite to amphibolite facies metamorphism and experienced pressures of 8.7 ± 1 kbar (~25–30 km depth) and temperatures between 465 ± 50 °C to 545 ± 75 °C [60,63] related to the mid-Cretaceous, regionally extensive west-vergent thrust system [7].

2.4. Blanchard River assemblage and Kluane Schist high-grade metamorphic rocks

The Blanchard River assemblage is juxtaposed along the southern margin of the Dezadeash

Formation (Figure 1). It consists mainly of penetratively deformed, interlayered quartz-biotite schist and quartz-biotite psammitic schist that grades eastward into proto-gneiss and paragneiss before becoming engulfed by the Ruby Range batholith (~64–54 Ma) of the Coast Plutonic Complex [19,26]. The Blanchard River assemblage is ~5000–6000 m thick and has a detrital zircon based maximum depositional age of 130–125 Ma [19]. The Dezadeash Formation, Blanchard River assemblage, and YCT are interpreted as a structural stack related to the mid-Cretaceous, regionally extensive west-vergent thrust system, although thrusting was somewhat diachronous (i.e., ~90 Ma in southeast Alaska compared to ~83–76 Ma in Yukon) [19,26]. The Blanchard River assemblage reached amphibolite facies metamorphism with P-T conditions estimated to have been ~6.5 kbars (~24 km depth) and ~640 °C [19,26].

The Kluane Schist is juxtaposed along the eastern margin of the Dezadeash Formation (Figure 1). It is a sequence of graphitic mica-chlorite-quartz schist and gneiss with a structural thickness of ~12,000 m that contains interfoliated bodies of serpentinized dunite up to 1.5 × 15 km in exposed dimensions [64]. Zircon geochronology indicates the protolith of the Kluane Schist is Late Cretaceous in age (<94 Ma) [17]. The Dezadeash Formation, Kluane Schist and YCT are also interpreted as a structural stack related to the mid-Cretaceous, regionally extensive west-vergent thrust system [17]. The Kluane Schist was subject to greenschist to amphibolite facies metamorphism with P-T estimated to have been 7–8 kbar (~24–30 km depth) and 500 °C [17,64,65].

2.5. Denali fault and Coast-Tatshenshini shear zone

The Denali fault system forms the western margin of the Dezadeash Formation (Figure 1). The Dezadeash Formation and Nutzotin Mountains sequence represent the same strata that was dismembered and displaced by the Denali fault system [45]. The Denali fault system is one of the main strike-slip faults in the Northern Cordillera, along which ~370 km of dextral slip occurred since the Early Cretaceous [66,67]. with the western boundary of the Coast Plutonic Complex is the Coast shear zone (Figure 1). The Coast shear zone extends more than 1000 km from southern British Columbia into southeastern Alaska [68–69]. Displacement across the Coast shear zone is dominantly east-over-west, and this occurred mainly in mid-Cretaceous time as part of the regionally extensive west-vergent thrust system [7,8,61,68–70]. Synkinematic tonalite sills intrude the western margin of the shear zone [61,68–72].

The Coast Shear zone was extended into southwest Yukon as part of the Tatshenshini shear zone (Figure 1) [73]. The Tatshenshini shear zone is characterized by phyllitic and protomylonitic to mylonitic turbidites of the Dezadeash Formation in the footwall and protomylonitic granodiorite of the Ruby Range Batholith (part of the Coast Plutonic Complex) in the hangingwall [73]. Kinematic indicators from the Dezadeash Formation and Ruby Range Batholith record a top-to-the southwest sense of shear that occurred in the Cretaceous.

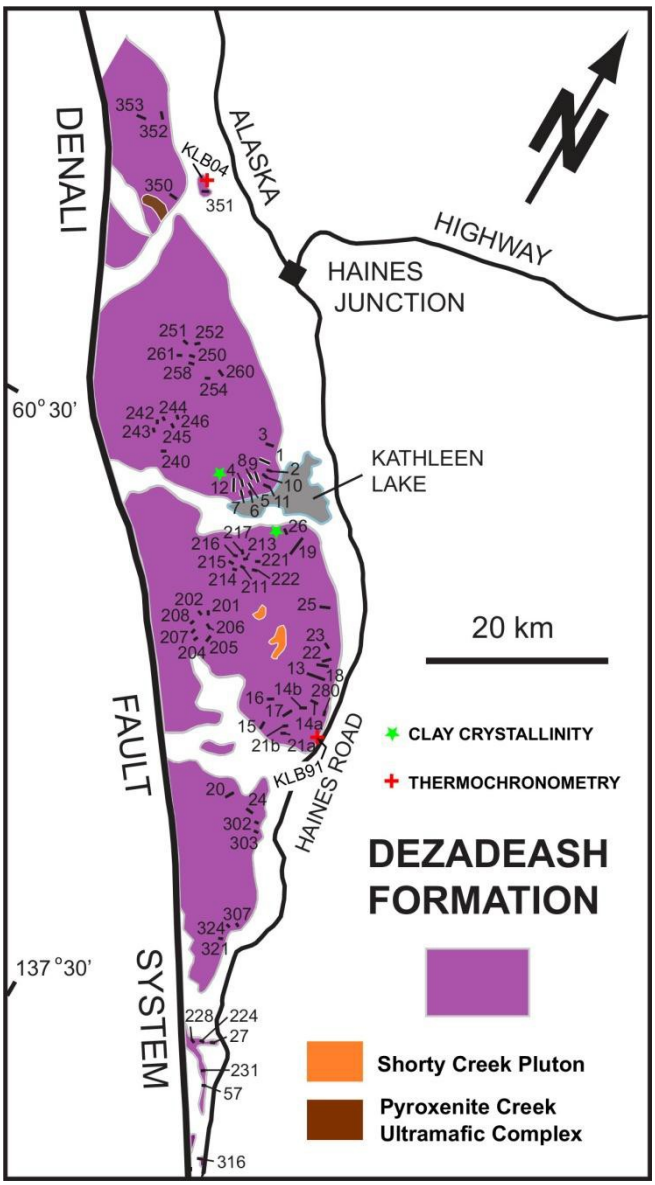

Figure 2. Location of measured sections (numbers) in the Dezadeash Formation, Yukon, from which samples were collected (individual sample locations are not shown: see Table 2). Also shown is the location of published thermochronometric data for the Dezadeash Formation (see Table 1 for details).

Table 2. Section locations (along which samples were collected), Dezadeash Formation, Yukon, Canada.

Section	NTS Map	Easting		Northing	Easting		Northing
1	115 A/11	Start	371000	6719500	End	369200	6718000
2	115 A/11	Start	371600	6718700	End	371200	6718600
3	115 A/11	Start	370400	6720800	End	369200	6720500
4	115 A/11	Start	369700	6716600	End	369200	6716200
5, 264	115 A/11	Start	369700	6716500	End	369400	6716700
6	115 A/11	Start	370500	6716300	End	370300	6716600
7	115 A/11	Start	369500	6715600	End	369300	6716000
8	115 A/11	Start	370300	6717000	End	369400	6717500
9	115 A/11	Start	370600	6717800	End	369800	6718300
10	115 A/11	Start	370900	6718300	End	370400	6718200
12	115 A/11	Start	369300	6715700	End	368500	6716700
13	115 A/11	Start	385400	6702500	End	383600	6702300
14A	115 A/11	Start	385500	6699300	End	384800	6699200
14B	115 A/11	Start	384700	6698800	End	384300	6698700
16	115 A/11	Start	381200	6698200	End	380700	6698200
17	115 A/11	Start	383300	6696900	End	384200	6697700
18	115 A/11	Start	385100	6703900	End	384100	6703800
19	115 A/11	Start	377000	6715000	End	376200	6714300
20	115 A/11	Start	382500	6687700	End	382300	6687300
21B	115 A/11	Start	384300	6695700	End	384300	6695700
22	115 A/11	Start	384700	7604600	End	384500	6705000
23	115 A/11	Start	384300	6705400	End	383800	6705900
24	115 A/11	Start	384700	6684700	End	384500	6684800
25	115 A/11	Start	382200	6709300	End	381400	6708700
26	115 A/11	Start	377200	6716300	End	382400	6715700
27, 224, 228	115 A/2	Start	392000	6665100	End	392000	6665100
28	115 A/2	Start	392100	6675100	End	392100	6676100
57, 231	A/2	Start	398000	6685100	End	398800	6688100
201–202	115 A/6	Start	371800	6701400	End	371800	6701400
203–206	115 A/6	Start	373800	6711400	End	372800	6711400

Continued on next page

Section	NTS Map	Easting		Northing	Easting		Northing
207–208	115 A/6	Start	371200	6701400	End	371200	6701400
211–217	115 A/6	Start	372200	6711400	End	372200	6711400
219–222	115 A/6	Start	373000	6708700	End	373000	6708700
240–246	115 A/12	Start	358200	6717500	End	358200	6717500
247	115 A/12	Start	359400	6717700	End	359400	6717700
250–252, 261	115 A/12	Start	358500	6725000	End	358500	6725000
254, 260	115 A/12	Start	361600	6724500	End	360700	6725300
257	115 A/12	Start	358600	6724700	End	358600	6724700
280, 74B, 400	116 A/6	Start	387094	6608552	End	387094	6608552
302–303	115 A/11	Start	381700	6634700	End	382500	6654800
307, 321, 324	115 A/11	Start	371700	6534700	End	352500	6554800
316	115 A/11	Start	374700	6674700	End	377500	6784800
350	115 A/12	Start	353956	6740958	End	352956	6740958
351, 74A	115 A/12	Start	352956	6740958	End	352956	6740958
352, 353	115 A/13	Start	344400	6745700	End	344300	6745800

3. Methods

This study is based on 16,335 m of measured strata from ~75 sections throughout the Dezadeash Formation (Figure 2, and Table 2). In addition to collecting standard bed-by-bed sedimentological measurements (i.e., bed thickness, lithology, grain size, and sedimentary structures), data was also collected pertaining to secondary deformation features (i.e., cleavage, folds, joints, and veins). Approximately 200 samples were collected from these sections, and a subset of samples representative of a wide range of lithologies were selected for a variety of analyses, including standard thin sections, X-ray diffraction, microfossils (palynomorphs and conodonts), and pyrolysis. Standard thin sections were prepared by Vancouver Petrographics Ltd. (Vancouver, British Columbia, Canada), and included sandstone (35), coquina (4), mudstone (11), hemipelagite (7), and tuff (15) samples. X-ray diffraction analysis was undertaken by AGAT Laboratories Ltd. (Calgary, Alberta, Canada) on a Siemens D5000 Bragg-Brentano diffractometer, and comprised sandstone (2), hemipelagite (1), and tuff (1) samples for quantitative X-ray diffraction analysis, including clay speciation, and scanning electron microscope (SEM) with energy dispersive X-ray spectroscopy (SEM-EDX) analyses. X-ray diffraction analysis was also performed by Activation Laboratories Ltd. (Ancaster, Ontario, Canada) on a Panalytical X'Pert Pro diffractometer, and consisted of mudstone (2) samples for quantitative XRD analysis, including clay speciation, the Rietveld method (i.e., whole pattern fitting) for determining the quantities of crystalline mineral phases, and determination of the Kübler Index (KI) and the Árkai Index (AI). Both KI and AI measure the "sharpness" of the diffractogram peaks; the sharpness of the peaks is an indication of the crystallinity of the clay minerals, which provides an indication of the extent of diagenesis and metamorphism [74,75].

Palynomorphs (spore and pollen) were prepared following standard extraction techniques [76], and included mudstone (4) and hemipelagite (4) samples. The degree of maturation of the palynomorphs was determined by visual comparison with the Thermal Alteration Index [77]. Conodonts were processed by the Geological Survey of Canada (Vancouver, British, Columbia, Canada), and only one limestone clast was analyzed. The degree of maturation of the recovered conodonts was determined by visual comparison with the Conodont Alteration Index [78]. Programmed temperature pyrolysis was performed by the Geological Survey of Canada (Calgary, Alberta, Canada) on a Rock-Eval 6 Turbo instrument, and comprised mudstone (12), hemipelagite (7), sandstone (1), phyllite (1), and mylonite (1) samples.

4. Results

4.1. Field relationships

Well-exposed outcrops of the Dezadeash Formation occur throughout the St. Elias Mountains in southwestern Yukon. The majority of the outcrops are dominated by thin- to thick-bedded sandstone-mudstone couplets that form packets up to ~335 m thick, and medium- to thick-bedded sandstone that form amalgamated units up to ~136 m thick. Well preserved primary sedimentary structures are common in these lithologies, including erosional structures (sole marks and small channels), depositional structures (graded bedding, planar-stratification, and cross-stratification), deformation structures (load and flame structures, convolute stratification, dish and pillar structures, and slump structures), and biogenic sedimentary structures comprising sparse bioturbation with few discrete trace fossils preserved in the interior of beds and on the soles of beds. Detailed descriptions of these sedimentary structures and their distribution are presented in [45] and [47,79]. The pristine nature of the sedimentary structures provided unambiguous evidence for the way-up of strata, and slump folds overlain by undeformed beds confirm that the slumps are due to soft-sediment movement and not a later tectonic deformation.

Superimposed on the primary sedimentary structures are a variety of secondary structures. Sandstone beds in thin- to medium-bedded sandstones-mudstone couplets locally display a sub-vertical parting (Figure 3A). The parting is spaced 5–30 cm apart with a mean spacing of ~10.2 cm. Parting planes are parallel to each other and can be traced from one sandstone bed into several overlying or underlying sandstone beds, but they are not present in thick-bedded sandstone beds. Although the parting resembles a poorly developed spaced cleavage, the mean ratio of the separation of the partings to the thickness of the beds (s/l) is ~0.95. According to [80], s/l > 0.05 belongs to a joint set.

Mudstones are characterized by a poorly developed parting or diagenetic foliation [cf. 81], which is sub-parallel to bedding (Figure 3B). The diagenetic foliation is moderately to strongly developed, parallel to curviplanar, and generally spaced 3–8 mm, although up to 20 mm spacing is also present. The diagenetic foliation is associated with a weakly to strongly developed spaced cleavage that is at a high-angle to bedding. The cleavage domains have a spacing of 5–85 mm and are smooth, occupy <1% of the rock volume and are parallel to curviplanar to each other. The intersection of the diagenetic foliation and spaced cleavage results in mudstones weathering into angular, irregularly-shaped pebble-sized clasts.

Rarely, well developed pencil structure is also present in the mudstone (Figure 3C) [81]. The pencil structure, formed by the intersection of well-developed diagenetic cleavage and spaced

cleavage (S_0-S_1), trends northwesterly. The pencil length varies from 49.5–164.2 mm and the width ranges from 2.25–11.25 mm, with a mean shape factor (length-to-width ratio, L/W) of 14.5. A plot of the length and width of the pencils suggests a shortening of 9–26% (Figure 4).

Locally, mudstones display a moderately to well-developed spaced cleavage [81]. The cleavage domains have a spacing of 1–5 mm and are smooth, occupy <1% of the rock volume and are parallel to each other (Figure 3D). The spaced cleavage appears to be roughly axial planar with north trending, upright tight folds that exhibit a fold height of several meters, but it is unclear if the folds belong to the oldest (F_1) or youngest (F_2) folds identified in the strata [45].

Hemipelagite beds display an irregular jointing spaced 10–20 cm (Figure 3E), resulting in the beds weathering into angular, block-shaped cobble-sized clasts. Volcaniclastic beds display a more regular jointing spaced 20–50 cm that is intersected by a very irregular second joint set that is sub-parallel to bedding (Figure 3F). As a result, the volcaniclastic beds weather into angular, irregularly-shaped boulder-sized clasts.

Several types of veins are locally present in the thin- to medium-bedded sandstones-mudstone couplets. The more common type of veining are swarms of veins that cross-cut bedding at various angles. The veins occur as differently oriented sets, often forming prominent networks, with sub-parallel veins regularly spaced ~10–20 cm. The veins are ~0.5–6 cm wide and syntaxial, with one or more phases of white quartz and minor amounts of calcite present that impart a banded appearance to the veins. Occasionally associated with the vein swarms are randomly oriented irregular vein masses, ptygma-like veins, and veinlets of milky white quartz. A less common type of veining are isolated veins and sets of veins parallel to bedding. The veins are ~4–8 cm wide and syntaxial, with a single phase of massive white quartz extending out from the wall rock of the vein.

4.2. Metamorphic mineral assemblages

Detailed petrography of the framework mode of sandstones and the petrography of volcaniclastic rocks (crystal and vitric tuffs) can be found in [48] and [82], respectively. Metamorphic minerals in the Dezadeash Formation were identified optically, utilizing procedures outlined in [83] for identifying phyllosilicate minerals, and with the aid of XRD analysis (Figure 5, and Table 3).

The dominant metamorphic mineral assemblage in sandstone is prehnite ± laumontite + chlorite + kaolinite + illite ± calcite, indicative of high temperature zeolite facies metamorphism [84]. Celadonite, pyrite, magnetite, and hematite were also observed in some thin sections. Prehnite was found in most of the thin sections and accounted for 10–50% of the thin section area. It occurs as individual grains and grain clusters that display sheaf-like structure and sweeping extinction, as well as cloudy, granular aggregates that form irregular poikilotopic patches replacing grains and matrix. Laumontite was noted in ~50% of the thin sections. It occurs as clear, irregular masses with distinct cleavage that forms poikilotopic patches replacing grains and as interstitial material. Calcite was observed in most of the thin sections. It occurs as specks of microspar in plagioclase, and as sparry cement replacing grains and grain interstices (up to 20% of the area in several thin sections). The sparry cement displays straight, thick Type II calcite twins and rare curved, thick Type III twins [cf., 85]. Type II calcite twins thick Type III twins were also observed in the coquina ("shell hash") thin sections, along with well developed microstyolites. In addition, the sandstone thin sections contain microveins of quartz-prehnite, calcite-prehnite, and calcite-quartz-prehnite, that in turn, are cross-cut by calcite microveins.

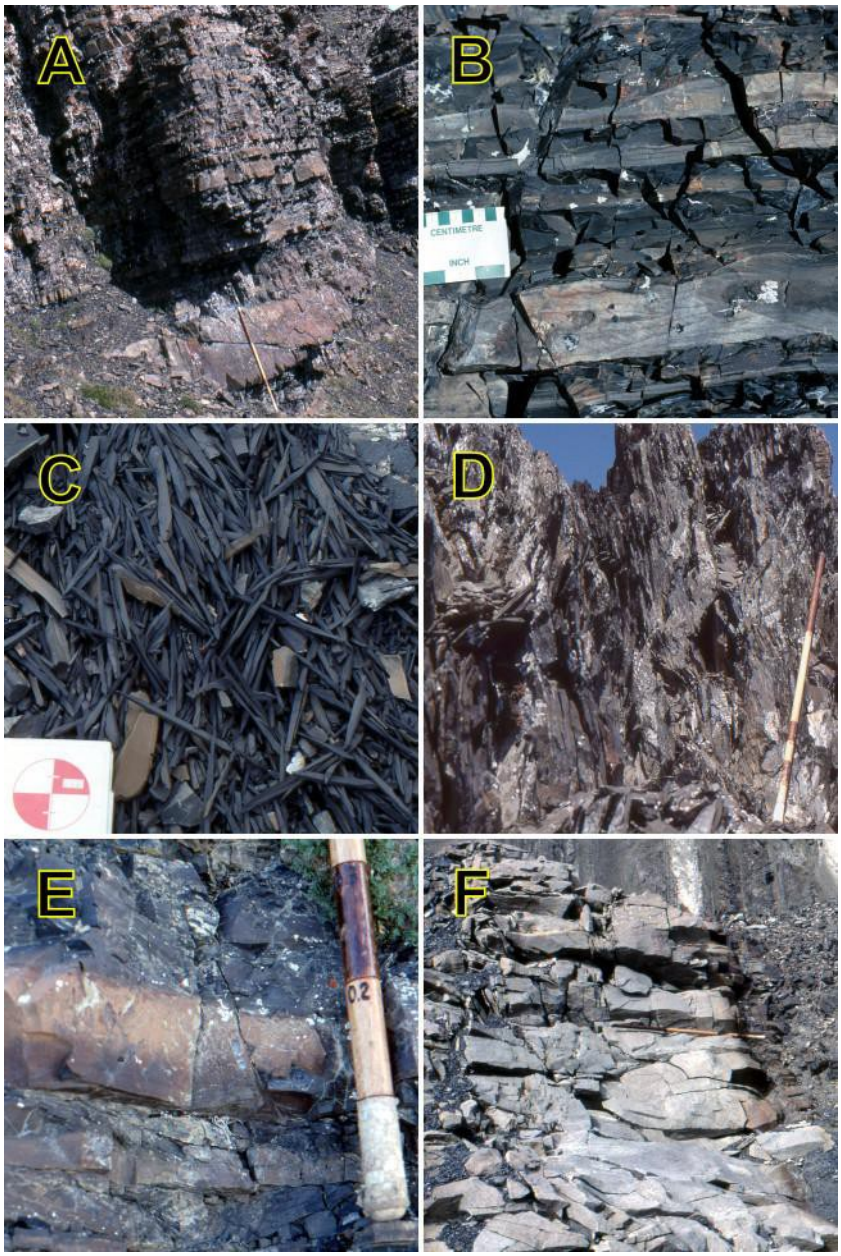

Figure 3. Photographs of representative secondary structures in the Dezadeash Formation, Yukon. (A) Parting (sub-vertical) in thin- to medium-bedded sandstone-mudstone couplets, 1.5 m long Jacob's Staff for scale. (B) Parting (sub-vertical) in thin-bedded sandstone-mudstone couplets, green squares at top of scale card are 1 cm long. (C) Pencil structure in mudstone, diameter of circle on notebook is 7 cm. (D) Spaced cleavage (vertical) in mudstone, 1.5 m long Jacob's Staff for scale. (E) Parting (vertical) in hemipelagite bed (brown bed), dark brown interval on Jacob's Staff is 0.1 m long. (F) Parting (horizontal) in tuff bed, 1.5 m long Jacob's Staff for scale.

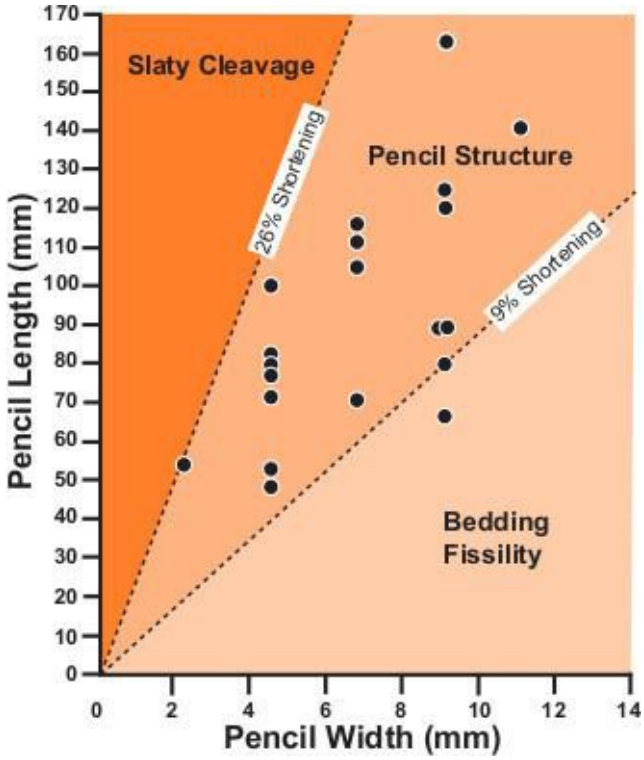

Figure 4. Plot of pencil width vs. length of mudstone samples from the Dezadeash Formation, Yukon [81].

The dominant metamorphic mineral assemblage in mudstone is quartz + albite + chlorite + illite ± calcite that is non-diagnostic for determining the metamorphic facies. Variably developed K-spar, stilpnomelane, and pyrite were also observed in some thin sections. Quartz, albite, chlorite, and illite, identified by XRD (<2 μm size fraction), likely form the irresolvable turbid matrix that is too fine grained to identify optically. Stilpnomelane was observed in ~50% of thin sections of mudstones exhibiting spaced cleavage. It occurs as small (~0.1 mm long), elongated crystals that are strongly pleochroic dark brown and pale brown, and lack the "bird's eye maple" texture present in biotite. Stilpnomelane shows varying degrees of preferred alignment, accounting for the foliation in the deformed mudstones. The hemipelagite thin sections also contain microveins of calcite-pyrite. The dominant metamorphic mineral assemblage in crystal tuff is similar to that of sandstone described previously. The dominant metamorphic mineral assemblage in vitric tuff is laumontite ± prehnite + illite + chlorite + kaolinite + quartz, indicative of high temperature zeolite facies metamorphism [84]. The abundance of illite suggests that tuff has been altered to a K-bentonite [86]. Variably developed albite, palagonite, and pyrite were also observed in some thin sections. Laumontite is ubiquitous in all of the thin sections (~70% by area). It occurs as clear, irregular masses with distinct cleavage that form poikilotopic patches replacing shards and interstitial material. Prehnite was found in ~50 % of the thin sections. It comprises cloudy, granular aggregates that form irregular poikilotopic patches replacing shards and interstitial material. Thin sections of vitric tuffs also show microveins of quartz,calcite, calcite + quartz, laumontite + quartz, and calcite + quartz + laumontite + prehnite.

Table 3. X-ray diffraction analyses, Dezadeash Formation, Yukon, Canada.

Sample	Lithology	Grain-size	Weight(%)	Quartz (%)	Plagioclase (%)	Kspar (%)	Calcite (%)	Muscovite (%)	Laumontite (%)	Siderite (%)	Kaolinite (%)	Chlorite (%)	Illite (%)	Other (%)	Clay Minerals (%)	Total (%)
25–3	Sandstone	Bulk (Coarse + Clay)	100.00	22	25	0	12	4	0	0	15	20	2		37	100
		Coarse(>2μm)	90.88	24	28	0	12	5	0	0	14	17	0		31	100
		Clay (<2μm)	9.12	2	2	0	4	0	0	0	25	53	14		92	100
400–3	Sandstone	Bulk Coarse	100.0094.9	24	37	0	2	2	0	0	11	15	9		34	100
		Clay	6	25	40	0	2	2	0	0	8	55	8		31	100
			5.04	1	1	0	0	0	0	0	51	35	12		98	100
1–3	Hemipelagite	Bulk	100.00	12	5 (Albite)	<0.1	63	2	0	0	8	8	2	Pyrite	18	100
		CoarseClay	96.00	13	5	<0.1	66	2	0	0	7	7	0	Bassanite	15	100
			4.00	0	0	0	6	0	0	0	24	20	50		94	100
264–1	Tuff	Bulk CoarseClay	100.00	37	7 (Albite)	0	6	3	41	3	0.5	0.5	2		2	100
			94.93	37	7	0	7	4	42	3	0	0	0		0	100
			5.07	4	2	0	1	0	33	0	8	8	44		60	100
12–5	Mudstone	Bulk CoarseClay	−	−	−	−	−	−	−	−	−	−	−	<10%	−	−
			−100	−29.8	−21.9 (Albite)	− <0.1	− 1.0	−	−	−	−0	−15.9	−15.3	expandable clay KI = 0.42, AI = 0.34Amorphous (16.1%)	−31.2	−100
26–1	Mudstone	Bulk CoarseClay	−	−	−	−	−	−	−	−	−	−	−	−	−	−
			−100	−20.9	−25.8 (Albite)	− 2.7	− 4.8	−0	−0	−0	−0	−18.8	− 7.5	KI = 0.26,AI = 0.33 Amorphous (19.5%)	−26.3	−100

Note: KI = Kübler Index (units of Δ°2θ); AI = Árkai Index (units of Δ°2θ).

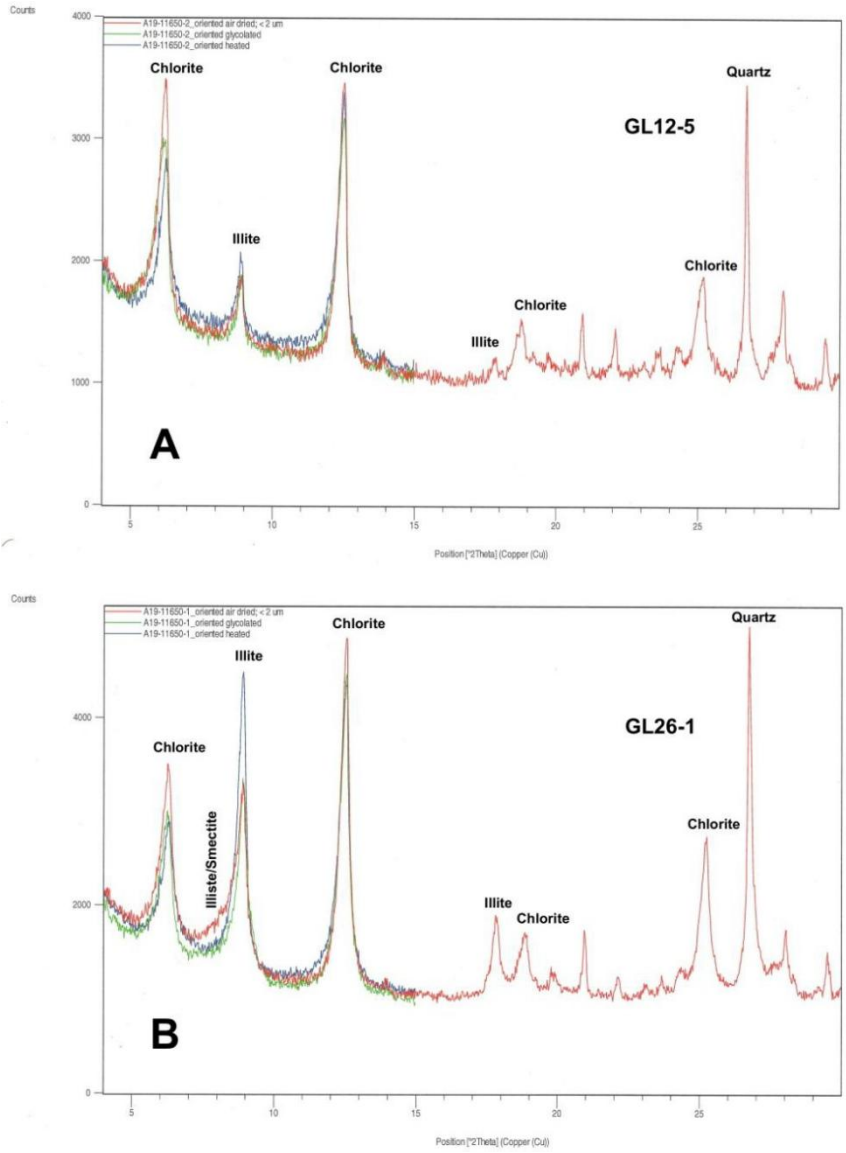

Figure 5. X-ray diffractograms of mudstone samples from the Dezadeash Formation, Yukon. (A) GL12–5. (B) GL26–1.

4.3. Metapeletic zones

The <2μm material analyzed in mudstone samples indicate that clay-size material consists mainly of albite, quartz, chlorite, and illite (the two-layer monoclinic polytype $2M_1$), minor amounts of calcite and K-feldspar, and rare interstratified illite/smectite (I/S) (Figure 6, and Table 3). In particular, sample GL12–5 displays <10% interstratified I/S characterized by long-range Reichweite ordering (i.e., R3). The KI for mudstone sample GL12–5 is 0.42 Δ°2θ, and the AI is 0.34 Δ°2θ, whereas for mudstone sample GL26–1, the KI is 0.26 Δ°2θ and the AI is 0.33 Δ°2θ. Three alteration zones have been defined based on the KI: diagenetic, with KI > 0.42 Δ°2θ; anchizone, with 0.42 Δ°2θ ≤ KI ≥ 0.25 Δ°2θ; and epizone, as KI <0.25 Δ°2θ [87,88]. The anchizone is transitional between diagenesis and metamorphism (i.e., the epizone). The diagenetic zone is further subdivided into shallow (KI > 1.0 Δ°2θ) and deep (1.0 Δ°2θ > KI > 0.42 Δ°2θ) subzones, and the anchizone is further subdivided into low (0.42 Δ°2θ < KI < 0.30 Δ°2θ) and high subzones (0.30 Δ°2θ < KI < 0.25 Δ°2θ) [89]. Boundaries

for the three main KI zones have also been designated according to AI values as diagenetic, with AI > 0.33 Δ°2θ; anchizone, with 0.33 Δ°2θ ≤ AI ≥ 0.26 Δ°2θ; and epizone, with AI < 0.26 Δ°2θ [75]. Note that KI and AI are defined such that the values decrease with increasing alteration. Mudstone samples from the Dezadeash Formation indicate deep diagenetic to high anchizone conditions according to KI and AI values.

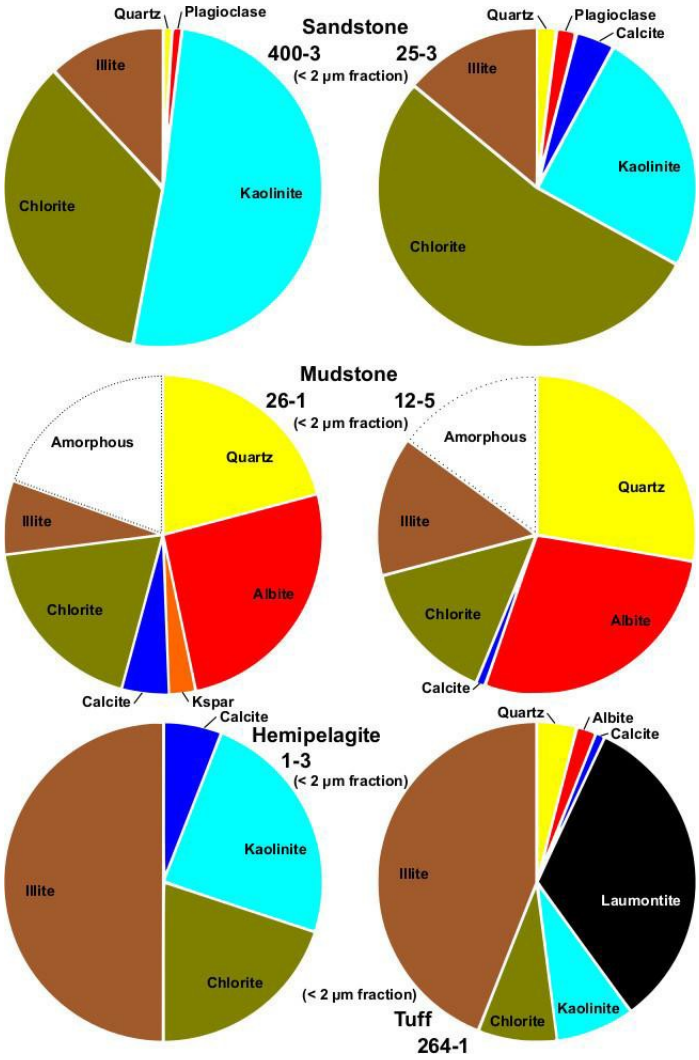

Figure 6. Pie diagrams of clay-size fraction (<2 µm) in sandstone, mudstone, hemipelagite, and tuff samples from the Dezadeash Formation, Yukon.

4.4. Thermal maturation stages

Preservation of palynomorphs extracted from the mudstone and hemipelagite samples is very poor (Table 4). Only an extremely sparse assemblage of dark brown to black, corroded silhouettes of what appear to be trilete spores, monosulcate pollen grains, and possibly one bisaccate pollen grain are present. The majority of the organic residue is dominated by palynodebris comprising: unstructured amorphous organic matter in the form of small (~20 µm), nearly equidimensional particles that are dark brown to black and semi-opaque or opaque ("black debris"); slightly larger (~50 µm), irregular "fluffy" masses appearing dark brown and partly translucent; minor amounts of dark brown globular masses

possibly representing degraded *Botryococcus* colonies; and rare dark brown to black phytoclasts (leaf cuticles ?) with no clear internal structure. The spore and pollen "wrecks" indicate a Thermal Alteration Index (TAI) of ~4.5. TAI is a semi-quantitative numerical scale from 1 to 5, with 1 being the lower maturity light color (i.e., colorless to light yellow) and 5 being the more mature darker color (i.e., black with indications of metamorphism) [77]. Hence, the TAI of ~4.5 for the Dezadeash Formation suggests mature thermal maturation.

Preservation of conodonts obtained from the limestone boulder is excellent (Table 5), and includes ramiform elements, *Neogondolella steinbergensis* (Mosher, 1968) and *Epigondolella bidentata* (Mosher 1968) indicating a Late Triassic (Late Norian) age. Also present are ichthyoliths, microbivalves, and foraminifers. The conodonts reveal a Conodont Alteration Index (CAI) of ~4–4.5: CAI is also a semi-quantitative numerical scale from 1 to 5, similar in principle to the TAI, with 1 corresponding to a lower maturity light color (i.e., clear or colorless) and 5 corresponding to a more mature darker color (i.e., black) [78]. Proposed alteration zones similar to the KI and AI zones include the diacaizone, with CAI < 4, ancaizone, with 4 ≥ CAI ≤ 5.5, and epicaizone, with CAI > 5.5, with increasing CAI values corresponding to increasing alteration [89]. Hence, the CAI of ~4–4.5 for the Dezadeash Formation suggests mature thermal maturation and ancaizone conditions.

All but one sample indicates a total organic carbon (TOC) content of <0.3 wt %, rendering the majority of the pyrolysis oven temperatures at which the maximum amounts of hydrocarbons are generated (T_{max}) as suspect (Table 6). Mudstone sample GL4–8 contains 1.26% TOC and has a corresponding T_{max} value of 589 °C. Three stages of thermal maturity with respect to oil source rocks have been designated as follows: immature, with T_{max} < 435 °C and attributed to diagenesis; mature (corresponding to the "oil window"), with T_{max} 435–470 °C and due to catagenesis (increasing pressure and temperature); and postmature, with T_{max} > 470 °C and indicative of metagenesis (i.e., incipient metamorphism) [90]. The one reliable sample is postmature, suggesting metagenesis conditions. Calculated parameters for this sample indicate a hydrogen index [HI = (S2/TOC) × 100] of HI = 5 and an oxygen index [OI = (S3/TOC) × 100, where S3 is the carbon dioxide generated during pyrolysis] of OI = 33, suggesting Type III (terrestrial) and IV (degraded or inert) kerogen is present. Type III kerogen is also indicated from the quantity of hydrocarbons generated by pyrolytic degradation (S2 = 0.06 mg of hydrocarbons/g of rock) and the TOC value of 1.26% when plotted on a graph of S2 versus TOC [91]. In summary, HI, OI, S2 and TOC parameters are in agreement with the type of organic matter recovered during the processing of samples for palynomorphs.

The extremely low TOC values discouraged the use of vitrinite reflectance analysis, perhaps the most widely utilized technique for determining thermal maturity of sedimentary rocks [92]. The percent reflectivity in oil (R_o) of vitrinite (a kerogen maceral) corresponds to the stage of thermal maturity: diagenesis, with R_o < 0.5 (also referred to as immature); catagenesis, with > 0.5 R_o< 1.3 (also referred to as mature with > 0.5R_o< 1.3, and postmature with > 1.3 R_o < 2); metagenesis, with > 2R_o< 4 (also referred to as overmature); and values of R_o > 4 are in the real of metamorphism [93,94]. Several correlations between T_{max} and R_o has been proposed [95,96]. The equation ln (% Rm) = (0.078 T_{max}) − 1.2 converts the T_{max} of 589 °C obtained from the Dezadeash mudstone sample to 3.8% Ro [95] and the equation Equivalent%R_o = (0.0165 T_{max}) − 6.5143 converts the mudstone T_{max} value of 589 °C to 3.2 [96]. The T_{max} value of the Dezadeash sample indicates a metagenesis stage of thermal maturation (i.e., overmature), and conversion of the T_{max} value to vitrinite reflectance values are consistent with the metagenesis conditions.

Table 4. Palynological analysis of mudstone and hemipelagites, Fezadeash Formation, Yukon, Canada.

Sample	Lithology	Spores	Pollen	AOM	Phytoclasts	Other
1–1	mudstone	Trilete, dark brown, corroded	Monosulcat e grain, dark brown, corroded	Black debris, round particles, dark brown to black, semi-opaqueor opaque; Irregular "fluffy" masses, dark brown and partlytranslucent; Globular masses, dark brown, degraded *Botryococcus* colonies?	Black phytoclasts	Pyrite
1–2	mudstone	Barren	Bisaccate grain, dark brown to black,corroded	black debris, round particles, dark brown to black, semi-opaqueor opaque; irregular 'fluffy' masses, dark brown and partly translucent		
1–3	mudstone	Barren	Monosulcate grain, black, corroded	black debris, round particles, dark brown to black, semi-opaqueor opaque		
1–4	mudstone	Trilete, dark brown, corroded	barren	black debris, round particles, dark brown to black, semi-opaqueor opaque; irregular "fluffy" masses, dark brown and partly translucent	black phytoclasts (leaf cuticles?)	
1–5	hemipelagite	Barren	Barren	black debris, round particles, dark brown to black, semi-opaqueor opaque; irregular "fluffy" masses; dark brown and partlytranslucent	black phytoclasts (leaf cuticles?)	pyrite
GL1–6	hemipelagite	Barren	Barren	black debris, round particles, dark brown to black, semi-opaqueor opaque		pyrite
GL1–7	hemipelagite	Barren	Barren	black debris, round particles, dark brown to black, semi-opaqueor opaque		
GL1–8	hemipelagite	Barren	Barren	black debris, round particles, dark brown to black, semi-opaqueor opaque		

Note: AOM = amorphous organic matter. Thermal Alteration Index (TAI) = ~4.5.

Table 5. Microfossil analysis of carbonate boulder, Dezadeash Formation, Yukon, Canada (modified from Orchard, 2000).

Sample	Fossils	Age	CAI
	ichthyoliths microbivalvesforaminifer conodonts: ramiform elements *Neogondolella steinbergensis* (Mosher, 1968)		
247–1	*Epigondolella bidentata* (Mosher 1968)	Late Triassic (Late Norian)	4–4.5

Table 6. Rock-Eval data, Dezadeash Formation, Yukon, Canada.

Sample	Lithology	TOC (wt%)	T_{max} (°C)	S_1 (mg HC/g rock)	S_2 (mg HC/g rock)	S_3 (mg CO_2/ g rock)	HI	OI
1–3	Hemipelagite	0.03	437	0.01	0.06	0.24	200	800
2–2	Hemipelagite	0.17	451	0.00	0.02	0.35	12	206
3–2	Hemipelagite	0.20	442	0.07	0.03	0.35	15	175
3–9	Hemipelagite	0.12	481	0.00	0.00	0.50	0	413
4–2	Hemipelagite	0.06	−40	0.01	0.00	0.21	0	350
4–7	Hemipelagite	0.15	285	0.16	0.03	0.36	20	240
4–8	Mudstone	1.26	589	0.04	0.06	0.41	5	33
8–5	Hemipelagite	0.08	362	0.01	0.00	0.23	0	288
9–4	Mudstone	0.15	342	0.00	0.00	0.35	0	233
9–6	Hemipelagite	0.17	406	0.01	0.00	0.54	0	318
12–4	Hemipelagite	0.10	428	0.01	0.00	0.38	5	380
12–5	Mudstone	0.19	314	0.12	0.01	0.28	0	147
16–1	Mudstone	0.14	−40	0.00	0.00	0.31	20	221
18–1	Sandstone	0.05	487	0.00	0.01	0.30	0	600
18–4	Hemipelagite	0.04	−40	0.00	0.00	0.42	0	1050
22–1	Mudstone	0.07	421	0.00	0.00	0.35	14	500
23–1	Sandstone	0.07	428	0.00	0.01	0.24	0	343
26–1	Hemipelagite	0.07	430	0.00	0.00	0.27	0	386
28–1	Phyllite	0.01	−40	0.00	0.00	0.28	0	2800
203–1	Mudstone	0.11	−40	0.00	0.00	0.30	0	273
210–1	Hemipelagite	0.25	433	0.00	0.00	0.27	0	108
213–1	Mudstone	0.08	−40	0.00	0.00	0.26	0	325
307–1	Mylonite	0.09	362	0.01	0.00	0.77	0	856

Note: TOC = total organic carbon; T_{max} = Rock-Eval oven temperature at maximum S_2 generation; S_1 = hydrocarbons thermally distilled from sample ("free hydrocarbons"); S_2 = hydrocarbons generated by pyrolytic degradation of kerogen in sample ("potential hydrocarbons"); S_3 = carbon dioxide generated during pyrolysis; HI = Hydrogen Index = (S_2x100/TOC); OI = Oxygen Index = (S_3x100/TOC); HC = hydrocarbons

5. Discussion

5.1. Metamorphic grade

Multidisciplinary analysis of various mineralogic and organic thermal indicators in rocks of diverse lithologies (e.g., sandstone, mudstone, hemipelagite, and tuff) from the Dezadeash Formation are summarized in a correlation diagram (Figure 7). In particular, secondary mineral assemblages in sandstone and tuff indicate subgreenschist, high temperature zeolite facies metamorphism; Kübler indices of illite and Árkai indices of chlorite in mudstone record diagenetic to high anchizone metapelitic conditions; the color of organic matter (i.e., Thermal Alteration Index of palynomorphs and Conodont Alteration Index) and the pyrolysis of organic matter and in mudstone and hemipelagite beds suggest that thermal maturation reached catagenesis to mesogenesis stages. Correlation of the various mineralogic and organic thermal indicators is internally consistent and suggests very low-grade metamorphism (VLGM) of the Dezadeash Formation. The development of an incipient slaty cleavage (i.e., S_0-S_1 pencil structure) in the Dezadeash Formation is also compatible with VLGM [99,100].

Note that on the correlation diagram, illite and chlorite crystallinities document slightly higher thermal alteration than metamorphic mineral assemblages, whereas organic matter records an even slightly higher thermal alteration than illite and chlorite crystallinities. This general trend of increasing thermal alteration from zeolite facies, to diagenesis-anchizone conditions, to catagenesis-mesogenesis stages is attributed to the various "phases" (i.e., hydrous Ca-Al silicates, sheet silicates, and organic matter) reacting at different rates, or kinetics [74,87,100]. The varying reaction kinetics imply that these out-of-equilibrium phases provide only qualitative estimates of paleopressure and paleotemperature [100–102].

Nonetheless, based on the combination of mineralogic and organic thermal indicators observed in the Dezadeash Formation (particularly the laumontite stability field, estimates of the P-T region for the zeolite facies, the diagenesis/anchizone boundary determined from fluid inclusion data, and the effective closure temperature of zircon fission tracks), a reasonable estimate for the maximum P-T conditions experience by the strata is 2.5 ± 0.5 kbar and 250 ± 25 ˚C (Figure 8). The estimated paleopressure corresponds to a depth of 7.6–11.4 km (assuming a rock density of $\rho = 2685$ kg/m^3). This depth is consistent with the observation of insipient spaced cleavage and widespread veining in the Dezadeash Formation, indicating that P-T conditions did not exceed the brittle-ductile transition zone that occurs at a depth of ~10–15 km and temperatures of ~250–350 °C [106].

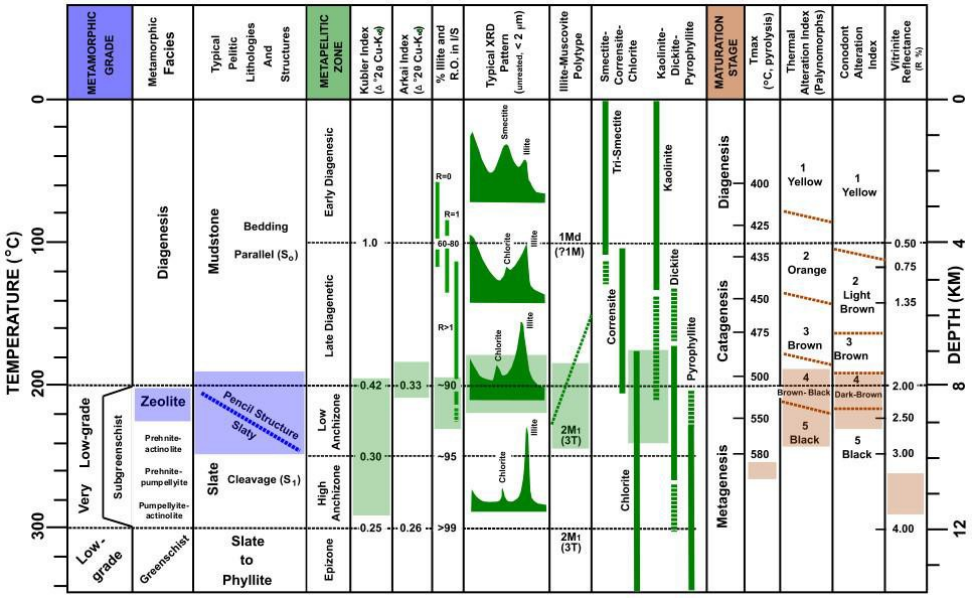

Figure 7. Correlation diagram of metamorphic grade, metapelitic zone, and maturation stage for the Dezadeash Formation, Yukon. Note that temperature and depth are only approximate [94,97,98].

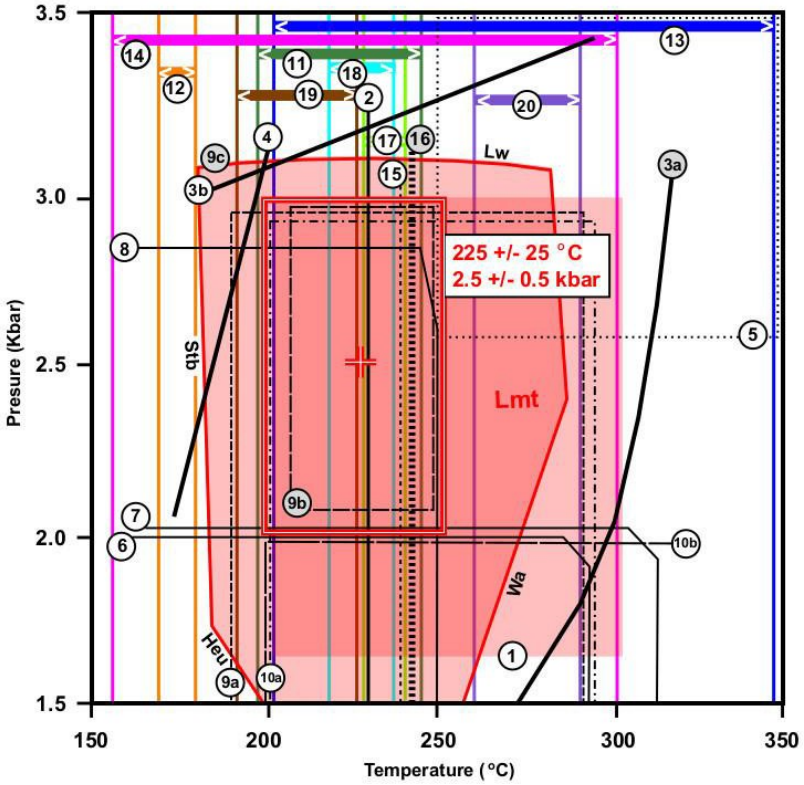

Figure 8. Estimate of P-T conditions experienced by the Dezadeash Formation, Yukon600 (Abbreviations are: Anorthite = An, Calcite = Cc, Chlorite = Chl, Heulandite = Heu, Lawsonite = Lw, Laumontite = Lmt, 601 Paragonite = Par, Prehnite = Pr, Quartz = Qz, Stilbite = Stb, Tremolite = Tr, Wairakite = Wa, Water = W).

Circled numbers refer to: 1) the zeolite facies metamorphism from 200–300 ˚C with total pressures below 3 kbar [83,103]; 2) the high temperature zeolite facies (i.e., Lmt with Pre) a temperature of around 230 ˚C [83]; 3a) the absence of wairakite suggests metamorphic conditions are limited by the Lmt-Wa for $P_{tot} = P_{CO2}$, specifically P < 3 kbars and T < 300 °C [104,105]; 3b) the absence of lawsonite suggests metamorphic conditions limited by the Lmt-Lw equilibrium for $P_{tot} = P_{CO2}$, specifically P < 3 kbars and T < 300 °C [104,105]; 4) the absence of heulandite suggests metamorphic conditions limited by the equilibrium of Heu = Lmt + Qz + W [83]; 5) the widespread veining of Qz ± Cc ± Lmt ± Pr suggests P-T conditions in the brittle ductile transition zone that occurs at 2.6–3.9 kbar (~10–15 km) and temperatures of ~250–350 ˚C [106]; 6) the laumontite dehydration equilibrium of Lmt = Wa + 2W at ~282 ± 5 ˚C and 2 kbar [107]; 7) the laumontite equilibrium of Lmt = An + 2Qz + 4W at 317 ± 10 ˚C and 2 kbar [108]; 8) the laumontite equilibrium of Lmt = Lw + 2Qz + 2W at 2.75 ± 0.25 kbar and 250 ˚C [108]; 9a)the laumontite stability field restricted to 180–285 ˚C at < 3 kbar in the NCASH system (Na_2O-CaO-Al_2O_2-SiO_2-H_2O) with excess H_2O and SiO_2 [109]; 9b) the zeolite facies between 210–250 ˚C at 2.1–2.9 kbar [109]; 9c) the stability field of laumontite with excess Qz + W [109]; 10a) the prehnite stability of 3Pr + Chl + 4Qz +18W = 4Heu + Tr between 200–280 ˚C and < 3 kbar [102]; 10b) the prehnite stability at T > 200 ˚C and P < 2 kbar for low XCO_2 [110]; 11) clay compositions containing 5–10% smectite in I/S interstratification corresponding to 200–250 ˚C [111]; 12) the R = 1 to R = 3 transition (i.e., short-range to long-range Rietveld ordering in I/S clay) at ~170–180 ˚C [112]; 13) the 1 M to 2 M polytypism transition in illite between 200–350 ˚C at ~2 kbar [113]; 14) straight thick Type II calcite twins developing in the range of 150–300 ˚C [114]; 15) the diagenesis/anchizone boundary at 240 ± 15 ˚C according to fluid inclusion data [115]; 16) the effective closure temperature (i.e., the temperature for 90% track retention) of zircon fissiontracks at ~240 ˚C [116]; 17) according to the formula $T_{peak} = [\ln(\%R_o) + 1.68]/0.0124$ for estimating maximum temperatures reached by vitrinite reflectance [95], calculated equivalent reflectance values of 3.2 and 3.8 for the Dezadeash Formation correspond to temperatures of 229 ˚C and 243 ˚C, respectively; 18) the diagram of nomograms of vitrinite reflectance vs. time and maximum temperature reveals that the calculated equivalent reflectance values of 3.2 and 3.8 correspond to temperatures between ~220–240 ˚C [117, their Figure 5]); 19) the Ahrrenius plot of temperature vs. time indicates the conodont CAI value of 4–4.5 for the Dezadeash Formation corresponds to a temperature of ~190–230 ˚C [78, their Figure 9]; and 20) the conodont CAI value of 4–4.5 for the Dezadeash Formation equates to a maximum temperature of 260–285 ˚C according to temperatures determined by Raman spectroscopy of carbonaceous material in conodont species [118].

5.2. Timing of metamorphism

The estimated maximum paleotemperature experienced by the Dezadeash Formation, together with published thermochronometric data for the strata, are plotted on a time vs. temperature diagram (Figure 9). The diagram shows that the Dezadeash Formation underwent relatively rapid, short-term heating followed by relatively gradual, long-term cooling. Based on a detrital zircon DA for Dezadeash Formation of 142 Ma [48], combined with a ZFT cooling age of ~110 Ma, strata reached peak metamorphic conditions between ~140–110 Ma. Hence the Dezadeash Formation appears to have been subject to metamorphism while the Blanchard River assemblage was being deposited (its detrital zircon maximum depositional age is 130–125 Ma) [19], and well before

deposition of the Kluane Schist (its detrital zircon maximum depositional age is 94 Ma) [17]. Furthermore, the estimated peak metamorphic conditions experienced by the Dezadeash Formation appear to have coincided with the decline of the Late Jurassic-Early Cretaceous Chitina arc (~160–140 Ma) [22,34–36], and rise of the Late Cretaceous Chisana arc (~120–105 Ma) [16,38].

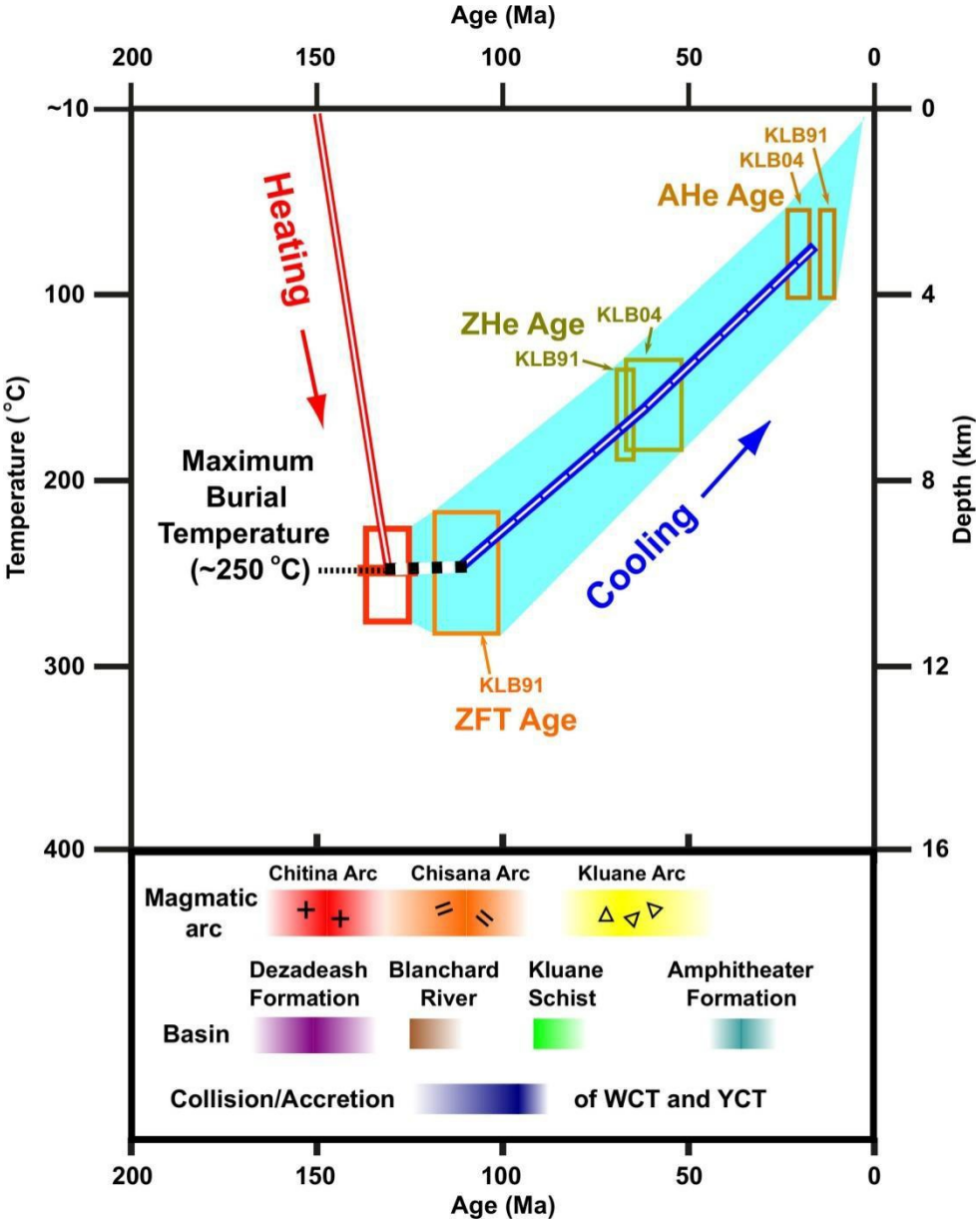

Figure 9. Time vs. temperature diagram for the Dezadeash Formation, Yukon. Thermochronometric samples KLB04 and KLB91 from [51]. Size of the boxes indicate uncertainties in age and temperature estimates.

5.3. Type of metamorphism

The lack of a well-developed penetrative deformation in the Dezadeash Formation suggests that burial metamorphism was responsible for the metamorphic conditions experienced by the strata [119]. The preserved compacted thickness of the Dezadeash Formation is ~3000 m. This thickness is comparable to the 3000 m thickness of the Nutzotin Mountains sequence (the proximal half of the

Dezadeash Formation) that rests unconformably on the WCT and is conformably overlain by the Chisana Formation [57]. Using a normal geothermal gradient of 25 ˚C/km [87], the base of the compacted Dezadeash Formation would have been subject to a temperature of only 75 ˚C. Furthermore, using an estimated present-day porosity (ϕ_N) for the strata of 0.05 and an inferred porosity when deposited (ϕ_O) of 0.4 based on the porosity of shaly-sand [120], and assuming that all changes in porosity with depth are the result of compaction [121], the calculated decompacted thickness of the Dezadeash Formation at the time of deposition (T_O), is ~4750 m. Again, using a normal geothermal gradient of 25 ˚C/km, the base of the decompacted Dezadeash Formation would have been subject to a temperature of only 118 ˚C. In addition, the stratigraphic relationship between the Dezadeash Formation and the Blanchard River assemblage is unknown [19]. Therefore, burial metamorphism seems an unlikely mechanism to account for the metamorphic grade of the Dezadeash Formation.

An alternative to burial metamorphism is "regional contact metamorphism". Regional contact metamorphism is caused by pluton intrusion and cooling over a large area, and is distinct from regional metamorphism and contact metamorphism [122,123]. This type of metamorphism has been widely recognized, and is commonly invoked for areas characterized by low grade metamorphism that lack penetrative fabrics, the presence of abundant closely spaced plutons, and an absence of a burial metamorphic mechanism [122,124–131]. The correspondence between peak metamorphic conditions experienced by the Dezadeash Formation and the existence of the Chitina and Chisana arcs suggests that regional contact metamorphism associated with coeval magmatism was a likely mechanism for metamorphism. In particular, plutonic roots of the Chitina arc are preserved as the Saint Elias plutonic suite in Yukon [37]. The Saint Elias plutonic suite has emplacement ages ranging from 160–130 Ma [37], with intrusions concentrated along the outboard margin of the WCT (corresponding to the axis of the Chitina arc, "C" in Figure 1). Plutonic roots of the Chisana arc are preserved as the Kluane Ranges plutonic suite and the Pyroxenite Creek complex in Yukon [37]. The Kluane Ranges plutonic suite and Pyroxenite Creek complex have emplacement ages between 117–106 Ma [37], with intrusions concentrated along the inboard margin of the WCT (corresponding to the axis of the Chisana arc, "A" in Figure 1). Thus, the very low-grade, subgreenschist, high temperature zeolite facies metamorphism experienced by Dezadeash Formation is attributed to regional contact metamorphism associated with emplacement of the Chitina and Chisana magmatic arcs.

5.4. Tectonometamorphic evolution and implications regarding the Northern Cordillera

The metamorphic event experienced by the Dezadeash Formation is clearly different from that preserved inthe Gravina sequence and Gravina belt in southeastern Alaska, and the Blanchard River assemblage and Kluane Schist in Yukon. Metamorphism of the Gravina sequence and Gravina belt is attributed to well documented northeast directed underthrusting of both units beneath the YCT in mid-Cretaceous time as a result of final accretion of the WCT to the North American margin [5,7,8,16,60,132–134], during which the Gravina sequence reached greenschist to amphibolite facies metamorphism [8], and the Gravina belt wassubject to zeolite to amphibolite facies metamorphism (with peak P-T conditions estimated to have been 8.7 ± 1 kbar, or ~25–30 km depth, and 465 ± 50 °C to 545 ± 75 °C [60,63]. Similarly, metamorphism of the Blanchard River assemblage and Kluane Schist are also attributed to northeast directed underthrusting of both units beneath the YCT in mid-Cretaceous time as a result of final accretion

of the WCT to the North American margin [17,19], during which the Blanchard River assemblage reached amphibolite facies metamorphism (with peak P-T conditions estimated to have been ~6.5 kbars, or ~24 km depth assuming a rock density of 2,750 kg/m^3, and ~640 °C) [19], and the Kluane Schist experienced greenschist to amphibolite facies metamorphism (with peak P-T conditions estimated to have been 7–8 kbar, or ~24–30 km depth, and 500 °C) [17,64]. Furthermore, there is no compelling evidence for underthrust Mesozoic flysch in the northern part of the Gravina-Nutzotin belt [13,14,64]. Thus, the Dezadeash Formation appears to have been subject to a temporally and spatially separate metamorphic event than that experienced by the Gravina Sequence, Gravina belt, Blanchard River assemblage, and Kluane Schist.

The diverse tectonometamorphic histories of the Dezadeash Formation in the northern part of the Gravina-Nutzotin belt, compared to that of the Gravina sequence and Gravina belt in the southern part of the Gravina-Nutzotin belt, and the Blanchard River assemblage and Kluane Schist, may be a manifestation oblique convergence and diachronous accretion of the WCT to the YCT [16,26–33, 135,136]. That is, underthrusting of the Gravina-Nutzotin belt decreases northward, coincident with a northward decrease in the timing of regionally extensive, mid-Cretaceous thrusting [26], suggesting that accretion of the WCT was south-to-north.

6. Conclusions

Multidisciplinary analysis of mineralogic and organic thermal indicators preserved in the Dezadeash Formation, Yukon, Canada, suggests that metamorphic mineral assemblages in sandstone and tuff indicate subgreenschist, high temperature zeolite facies metamorphism; Kübler indices of illite and Árkai indices of chlorite in mudstone record diagenetic to high anchizone metapelitic conditions; and the color of organic matter (i.e., Thermal Alteration Index of palynomorphs and Conodont Alteration Index) and pyrolysis of organic matter in mudstone and hemipelagite beds show that thermal maturation reached catagenesis to mesogenesis stages.

Based mainly on published estimates for the laumontite stability temperature, the P-T region for the zeolite facies, the temperature of the diagenesis/anchizone boundary, and the effective closure temperature of zircon fission tracks, a reasonable estimate for the maximum P-T conditions experienced by the Dezadeash Formation are 2.5 ± 0.5 kbar and 250 ± 25 ˚C. The estimated paleopressure corresponds to a burial depth of 7.6–11.4 km. The estimated maximum paleotemperature experienced by the Dezadeash Formation, together with published thermochronometric data for the strata, shows that the Dezadeash Formation underwent relatively rapid, short-term heating followed by relatively gradual, long-term cooling between 140–110 Ma, attributed to regional scale contact metamorphism related to emplacement of the Jurassic-Cretaceous Chitina and Chisana magmatic arcs.

The tectonometamorphic history of the Dezadeash Formation is inconsistent with previous reconstructions of the deformation and crustal-scale structure of the Northern Cordillera that posit 756 the Dezadeash Formation was thrust to depths > 20 km beneath the Blanchard River assemblage, Kluane Schist, and YCT in the mid-Cretaceous. The tectonometamorphic history of the Dezadeash Formation also contrasts sharply with the Gravina belt and Gravina sequence in the southeastern Alaska that were apparently underthrust (~25–30 km) beneath the YCT along a regional extensive, mid-Cretaceous west-vergent thrust system. The diverse tectonometamorphic histories of the Dezadeash Formation in the northern part of the Gravina-Nutzotin belt, compared to that

of the Gravina sequence and Gravina belt in the southern part of the Gravina-Nutzotin belt, may be a manifestation oblique convergence and diachronous northward accretion of the WCT to the Mesozoic margin of North America.

Acknowledgements

I wish to acknowledge that field work was undertaken in the traditional territory of the Champagne and Aishihik First Nations. Aaron Ogden, Marty Mossop, and Werner Liebau are thanked for providing field assistance in the early phases of this project. Past discussions with Stephen Johnston regarding the "Dezadeash molasse" were always entertaining. Terry Pavlis and Branimir Sergvic are thanked for their insightful comments on an earlier version of the manuscript, and two anonymous reviewers are also thanked for their helpful comments on the revised manuscript. The author declares there are no competing interests and no specific funding for this work.

Conflict of interest

The author declare no conflict of interest.

References

1. Tipper HW, Wheeler JO, McFeely P (1991) Tectonic assemblage map of the Canadian Cordillera and adjacent parts of the United States of America. *Geol Surv Can Map*.
2. Nelson JL, Colpron N, Israel D (2013) The cordillera of British Columbia, Yukon, and Alaska: tectonics and metallogeny. *Spec Publ Soc Econ Geol* 17: 53–110.
3. Monger JWH (2014) Logan medallist 1. Seeking the suture: The Coast-Cascade conundrum. *Geosci Can* 41: 379–398.
4. Berg HC, Jones DL, Richter DH (1972) Gravina-Nutzotin belt—tectonic significance of an Upper Mesozoic sedimentary and volcanic sequence in southern and southeastern Alaska. *U S Geol Surv Prof Pap* 800D: D1–D24.
5. Crawford ML, Hollister LS, Woodsworth GJ (1987) Crustal deformation and regional metamorphism across a terrane boundary, Coast Plutonic complex, British Columbia. *Tectonics* 6: 343–361.
6. Gehrels GE, McClelland WC, Samson SD, et al. (1990) Ancient continental margin assemblage in the northern Coast Mountains, southeast Alaska and northwest Canada. *Geology* 18: 208–211.
7. Rubin CM, Saleeby JB, Cowan DS, et al. (1990) Regionally extensive mid-Cretaceous west-vergent thrust system in the northwestern Cordillera: implications for continent-margin tectonism. *Geology* 18: 276–280.
8. Rubin CM, Saleeby JB (1992) Thrust tectonics and Cretaceous intracontinental shortening in southeast Alaska. *Thrust Tectonics,* Springer, Dordrecht.
9. Stanley WD, Labson VF, Nokleberg WJ, et al. (1990) The Denali fault system and Alaska Range of Alaska: Evidence for underplated Mesozoic flysch from magnetotelluric surveys. *Geol Soc Am Bull* 102: 160–173.

10. Beaudoin BC, Fuis GS, Mooney WD, et al. (1992) Thin, low-velocity crust beneath the southern Yukon-Tanana terrane, east-central Alaska: Results from Trans-Alaska crustal transect refraction/wide-angle reflection survey. *J Geophys Res* 97: 1921–1941.
11. McClelland WC, Gehrels GE, Saleeby JB (1992) Upper Jurassic-Lower Cretaceous basinal strata along the Cordilleran margin: implications for the accretionary history of the Alexander-Wrangellia-Peninsular terrane. *Tectonics* 11: 823–835.
12. Mathez EA, Duba AG, Peach CL, et al. (1995) Electrical conductivity and carbon in metamorphic rocks of the Yukon-Tanana Terrane, Alaska. *J Geophys Res* 100: 187–196.
13. Fisher MA, Pellerin L, Nokleberg WJ, et al. (2007) Crustal structure of the Alaska Range orogen and Denali fault along the Richardson Highway. *Geol Soc Am Spec Pap* 431: 43–53.
14. Aleinkoff JN, Farmer GL, Rye RO, et al. (2000) Isotopic evidence for the sources of Cretaceous and Tertiary granitic rocks, east-central Alaska: Implications for the tectonic evolution of the Yukon-Tanana terrane. *Can J Earth Sci* 37: 945–956.
15. Johnston ST, Canil D (2007) Crustal structure of SW Yukon, northern Cordillera: implications for crustal growth in a convergent margin orogen. *Tectonics* 26: 1–18.
16. Trop JM, Ridgway KD (2007) Mesozoic and Cenozoic tectonic growth of southern Alaska: a sedimentary basin perspective. *Geol Soc Am Spec Pap* 421: 55–94.
17. Stanley B (2012) Structural geology and geochronology of the Kluane Schist, southwest Yukon Territory. Waterloo, Ontario: University of Waterloo. Available from: http://hdl.handle.net/10012/7096.
18. Hildebrand RS (2013) Mesozoic assembly of the North American Cordillera. *Geol Soc Am Spec Pap* 495.
19. Vice L (2017) Late Cretaceous to Paleocene evolution of the Blanchard River assemblage, southwest Yukon: implications for Mesozoic accretionary processes in the northwestern Cordillera. Burnaby, British Columbia: Simon Fraser University.
20. Monger JWH, Journeay JM (1994) Guide to the geology and tectonic evolution of the southern Coast Mountains. *Geol Surv Can Open File* 2490.
21. Plafker G, Berg HC (1994) Overview of the geology and tectonic evolution of Alaska. *The Geology of Alaska.* Geological Society of America, Geology of North America, 989–1021.
22. Nokleberg WJ, Plafke, G, Wilson FH (1994) Geology of south-central Alaska. *The Geology of Alaska*. Geological Society of America, Geology of North America, 311–366.
23. Clift PD, Draut AE, Kelemen PB, et al. (2005) Stratigraphic and geochemical evolution of an oceanic arc upper crustal section: The Jurassic Talkeetna Volcanic Formation, south-central Alaska. *Geol Soc Am Bull* 117: 902– 925.
24. Beranek LP, van Staal CR, McClelland WC, et al. (2014) Late Paleozoic assembly of the Alexander-Wrangellia-Peninsular composite terrane, Canadian and Alaskan Cordillera. *Geol Soc Am Bull* 126: 1531–1550.
25. Greene AR, Scoates JS, Weis D, et al. (2010) The architecture of oceanic plateaus revealed by the volcanic stratigraphy of the accreted Wrangellia oceanic plateau. *Geosphere* 6: 47–73.
26. Vice L, Gibson HD, Israel D (2020) Late Cretaceous to Paleocene tectonometamorphic evolution of Blanchard River assemblage, southwest Yukon: New insight into the terminal accretion of Insular terranes in the Northern Cordillera. *Lithosphere*.
27. Pavlis TL (1982) Origin and age of the Border ranges fault of southern Alaska and its bearing on the late Mesozoic tectonic evolution of Alaska. *Tectonics* 1: 343–368.

28. Pavlis TL (1989) Middle Cretaceous orogenesis in the northern Cordillera: A Mediterranean analog of collision-related extensional tectonics. *Geology* 17: 947–950.
29. Ridgway KD, Trop JM, Nokleberg WJ, et al. (2002) Mesozoic and Cenozoic tectonics of the eastern and central Alaska Range: Progressive basin development and deformation in a suture zone. *Geol Soc Am Bull* 114: 1480–1504.
30. Pavlis TL, Amato JM, Trop JM, et al. (2019) Subduction polarity in ancient arcs: A call to integrate geology and geophysics to decipher the Mesozoic tectonic history of the northern Cordillera of North America. *GSA Today* 29: 4–10.
31. Pavlis TL, Amato JM, Trop JM, et al. (2020) Subduction Polarity in Ancient Arcs: A Call to Integrate Geology and Geophysics to Decipher the Mesozoic Tectonic History of the Northern Cordillera of North America: REPLY. *GSA Today* 30: 51–58.
32. Clennett EJ, Sigloch K, Mihalynuk MG, et al. (2020) A quantitative tomotectonic plate reconstruction of western North America and the eastern Pacific Basin. *Geochem Geophys Geosyst* 21.
33. Sigloch K, Mihalynuk MG (2020) Comment on GSA Today article by Pavlis et al., 2019: "Subduction Polarity in Ancient Arcs: A Call to Integrate Geology and Geophysics to Decipher the Mesozoic Tectonic History of the Northern Cordillera of North America". *GSA Today* 30: 47–50.
34. Plafker G, Nokleberg WJ, Lull JS (1989) Bedrock geology and tectonic evolution of the Wrangellia, Peninsular, and Chugach terranes along the trans-Alaska crustal transect in the Chugach Mountains and southern Copper River basin, Alaska. *J Geophys Res Solid Earth* 94: 4255–4295.
35. Roeske SM, Pavlis TL, Snee LW, et al. (1991) 40Ar/39Ar isotopic ages from the combined Wrangellia-Alexander terrane along the Border Ranges fault system in the eastern Gugach Mountains and Glacier Bay, Alaska. Geologic Studies in Alaska by the United States Geological Survey 1990: 180–195.
36. Roeske SM, Snee LW, Pavlis TL (2003) Dextral-slip reactivation of an arc-forearc boundary during Late Cretaceous–Early Eocene oblique convergence in the northern Cordillera. *Geol Soc Am Spec Pap* 371: 141–170.
37. Dodds CJ, Campbell RB (1988) *Potassium-argon ages of mainly intrusive rocks in the Saint Elias Mountains, Yukon and British Columbia.* Geological Survey Canada Paper.
38. Short EJ, Snyder DC, Trop JM, et al. (2005) New findings on Early Cretaceous volcanism within the allochthonous Wrangellia terrane, south-central Alaska: Stratigraphic, geochronologic, and geochemical data from the Chisana Formation, Nutzotin Mountains. *Geol Soc Am Abstr Programs* 37: 81.
39. Sturrock DL, Armstrong RL, Maxwell RB (1980) Age and Sr isotope composition of the Pyroxenite Creek ultramafic complex, southwestern Yukon Territory: An Alaskan-type ultramafic intrusion. *Geol Surv Can Curr Res Pap* 80–1B: 185–188.
40. Nokleberg WJ, Parfenov WJ, Monger JWH, et al. (2000) Phanerozoic Tectonic Evolution of the Circum-North Pacific. *U S Geol Surv Prof Pap* 1626.
41. Amato JM, Rioux ME, Kelemen PB, et al. (2007) U-Pb geochronology of volcanic rocks from the Jurassic Talkeetna Formation and detrital zircons from prearc and postarc sequences: Implications for the age of magmatism and inheritance in the Talkeetna arc. *Geol Soc Am Spec Pap* 431: 253–271.

42. Armstrong RL (1988) Mesozoic and Early Cenozoic Magmatism of the Canadian Cordillera. *Geol Soc Am Spec Pap* 218: 55–92.
43. Gehrels GE, Rusmore M, Woodsworth G, et al. (2009) U-Th-Pb geochronology of the Coast Mountains batholith in north coastal British Columbia: Constraints on age and tectonic evolution. *Geol Soc Am Bull* 121: 1341–1361.
44. Eisbacher GH (1985) Pericollisional strike-slip faults and synorogenic basins, Canadian Cordillera. *Spec Publ Soc Econ Paleontol Mineral* 37: 265–282.
45. Eisbacher GH (1976) Sedimentology of the Dezadeash flysch and its implications for strike- slip faulting along the Denali fault, Yukon Territory and Alaska. *Can J Earth Sci* 13: 1495–1513.
46. Lowey GW (1992) Variation in bed thickness in a turbidite succession, Dezadeash Formation (Jurassic-Cretaceous), Yukon, Canada: Evidence of thinning-upward and thickening-upward cycles. *Sediment Geol* 78: 217–232.
47. Lowey GW (2007) Lithofacies analysis of the Dezadeash Formation (Jura-Cretaceous), Yukon, Canada: The depositional architecture of a mud/sand-rich turbidite system. *Sediment Geol* 198: 273–291.
48. Lowey GW (2019) Provenance analysis of the Dezadeash Formation (Jurassic-Cretaceous), Yukon, Canada: Implications regarding a linkage between the Wrangellia composite terrane and the western margin of Laurasia. *Can J Earth Sci* 56.
49. Dodds CJ, Campbell RB (1992) Overview, legend and mineral deposit tabulations for Geology of southwest Kluane Lake map area (115G and F[E1/2]), Yukon Territory, Open File 2188; Geology of Mount St. Elias map area (115B and C[E1/2]), Yukon Territory, Open File 2189; Geology of southwest Dezadeash map area (115A), Yukon Territory, Open File 2190; and Geology of northeast Yakutat Map Area (114O) and Tatshenshini River (114 P) map areas. *Geol Surv Can Open File* 2191.
50. Ridgway KD, Sweet AR (1995) Climatically induced floristic changes across the Eocene-Oligocene transition in the northern high latitudes, Yukon Territory, Canada. *Geol Soc Am Bull* 107: 676–696.
51. Enkelmann E, Piestrzeniewicz A, Falkowski S, et al. (2017) Thermochronology in southeast Alaska and southwest Yukon: Implications for North American plate response to terrane accretion. *Earth Planet Sci Lett* 457: 348–358.
52. Brandon MT, Vance JA (1998) Fission-track ages of detrital zircon grains: Implications for the tectonic evolution of the Cenozoic Olympic subduction complex. *Am J Sci* 292: 565–636.
53. Peyton LS, Carrapa B (2013) An introduction to low-temperature thermochronologic techniques, methodology, and applications. *Am Assoc Pet Geol Stud Geol* 65: 15–36.
54. McDermott RG, Ault AK, Caine JS, et al. (2019) Thermotectonic history of the Kluane Ranges and evolution of the eastern Denali fault zone in southwestern Yukon, Canada. *Tectonics* 38: 2983–3010.
55. Richter DH (1976) Geologic map of the Nabesna Quadrangle, Alaska. *U S Geol Surv Misc Invest Ser Map*.
56. Kozinski J (1985) Sedimentology and tectonic significance of the Nutzotin mountains sequence, Alaska. Albany, New York: State University of New York.
57. Manuszak JD, Ridgway KD, Trop JM, et al. (2007) Sedimentary record of the tectonic growth of a collisional continental margin: Upper Jurassic-Lower Cretaceous Nutzotin Mountains sequence, eastern Alaska Range, Alaska. *Geol Soc Am Spec Pap* 431:345–377.

58. Manuszak JD, Ridgway KD (2000) Stratigraphic architecture of the Upper Jurassic–Lower Cretaceous Nutzotin Mountains sequence, Nutzotin and Mentasta Mountains, Alaska. *Alaska Div Geol Geophys Surv Prof Rep* 119: 63–75.
59. Rubin CM, Saleeby JB (1991) The Gravina Sequence: Remnants of a Mid-Mesozoic oceanic arc in southern southeast Alaska. *J Geophys Res Solid Earth* 96: 14551–14568.
60. McClelland WC, Anovitz LM, Gehrels G (1991) Thermobarometric constraints on the structural evolution of the Coast Mountains batholith, central southeastern Alaska. *Can J Earth Sci* 28: 912–928.
61. McClelland WC, Gehrels GE, Samson SD, et al. (1992) Protolith relations of the Gravina Belt and Yukon–Tanana terrane in central southeastern Alaska. *J Geol* 100: 107–123.
62. Gehrels GE (2000) Reconnaissance geology and U-Pb geochronology of the western flank of the Coast Mountains between Juneau and Skagway, southeastern Alaska. *Geol Soc Am Spec Pap* 343: 213–233.
63. Cohen HA, Lundberg N (1993) Detrital record of the Gravina arc, southeastern Alaska: petrology and provenance of Seymour Canal Formation sandstones. *Geol Soc Am Bull* 105: 1400–1414.
64. Mezger JE, Chacko T, Erdmer P (2001) Metamorphism at a late Mesozoic accretionary margin: a study from the Coast Belt of the North American Cordillera. *J Metamorp Geol* 19: 121–137.
65. Tempelman-Kluit DJ (1976) The Yukon Crystalline terrane: Enigma in the Canadian Cordillera. *Geol Soc Am Bull* 87: 1343–1357.
66. Clague JJ (1979) The Denali fault system in southwest Yukon Territory—A geologic hazard? *Geol Surv Can Pap* 79-1A: 169–178.
67. Lowey GW (1998) A new estimate of the amount of displacement on the Denali Fault system based on the occurrence of carbonate megaboulders in the Dezadeash Formation (Jura-Cretaceous), Yukon, and the Nutzotin Mountains sequence (Jura-Cretaceous), Alaska. *Bull Can Pet Geol* 46: 379–386.
68. Andronicos CL, Hollister LS, Davidson C, et al. (1999) Kinematics and tectonic significance of transpressive structures within the Coast Plutonic Complex, British Columbia. *J Struct Geol* 21: 229–243.
69. Chardon D, Andronicos CL, Hollister LS (1999) Large-scale shear zone patterns and displacements within magmatic arcs: The Coast Plutonic Complex, British Columbia. *Tectonics* 18: 278–292.
70. Stowell HH, Hooper RJ (1990) Structural development of the western metamorphic belt adjacent to the Coast Plutonic Complex: Evidence from Holkham Bay. *Tectonics* 9: 391–407.
71. Ingram GM, Hutton DHW (1994) The Great Tonalite Sill: Emplacement into a contractional shear zone and implications for Late Cretaceous to early Eocene tectonics in southeastern Alaska and British Columbia. *Geol Soc Am Bull* 106: 715–728.
72. Klepeis KA, Crawford ML, Gehrels G (1998) Structural history of the crustal-scale Coast shear zone north of Portland, southeast Alaska and British Columbia. *J Struct Geol* 20: 883–904.
73. Lowey GW (2000) The Tatshenshini shear zone (new) in southwestern Yukon, Canada: Comparison with the Coast shear zone in British Columbia and southeastern Alaska and implications regarding the Shakwak suture. *Tectonics* 19: 512–528.

74. Kisch HJ (1987) Correlation between indicators of very low-grade metamorphism. *Low Temp Metamorph* 227–300.
75. Árkai P (1991) Chlorite crystallinity: an empirical approach and correlation with illite crystallinity, coal rank and mineral facies as exemplified by Palaeozoic and Mesozoic rocks of northeast Hungary. *J Metamorp Geol* 9: 723–734.
76. Traverse A (1988) *Paleopalynology,* Unwin Hyman: New York.
77. Staplin FL (1969) Sedimentary organic matter, organic metamorphism, and oil and gas occurrence. *Bull Can Pet Geol* 17: 47–66.
78. Lowey GW (1980) Depositional themes in a turbidite succession, Dezadeash Formation (Jura-Cretaceous), Yukon. Calgary, Alberta: University of Calgary.
79. Hancock PL (1982) Distinction between cleavage and joint using fracture separation. *Atlas of deformational and metamorphic rock fabrics, Springer-Verlag*, New York, 186–187.
80. Passchier CW, Trouw RAJ (1996) *Micro-tectonics*. Springer-Verlag: New York.
81. Lowey GW (2011) Volcaniclastic gravity flow deposits in the Dezadeash Formation (Jura-Cretaceous), Yukon, Canada: Implications regarding the tectonomagmatic evolution of the Chitina arc in the northern Cordillera of North America. *Lithos* 125: 86–100.
82. Folk RL (1974) *Petrology of sedimentary rocks*. Hemphill Publishing Company, Austin, Texas.
83. Liou JG, Maruyama S, Cho M (1987) Very low-grade metamorphism of volcanic and volcaniclastic rocks- mineral assemblages and mineral facies. *Low Temp Metamorph* 59–113.
84. Weber JC, Ferrill DA, Roden-Tice MK (2001) Calcite and quartz microstructural geothermometry of low-grade metasedimentary rocks, Northern Range, Trinidad. *J Struct Geol* 23: 93–112.
85. Huff WD (2016) K-bentonites: A review. *Am Mineral* 101: 43–70.
86. Blenkinsop TG (1988) Definition of low-grade metamorphic zones using illite crystallinity. *J Metamorp Geol* 6: 623–636.
87. Merriman RJ, Frey M (1999) Patterns of very low-grade metamorphism in metapelitic rocks. *Low-grade metamorphism.* Osney Mead, Oxford, 61–107.
88. Valín ML, García -López S, Brime C, et al. (2016) Tectonothermal evolution in the core of an arcuate fold and thrust belt: the south-eastern sector of the Cantabrian Zone (Variscan belt, north-western Spain). *Solid Earth* 7: 1003–1022.
89. García-López S, Bastida F, Aller J, et al. (2001) Geothermal palaeogradients and metamorphic zonation rom the conodont colour alteration index (CAI). *Terra Nova* 13: 79–83.
90. Peters KE, Casa MR (1994) Applied source rock geochemistry. *Am Assoc Pet Geol Mem* 60: 93–120.
91. Langford FF, Blanc-Valleron M (1990) Interpreting rock-eval pyrolysis data using graphs of pyrolizable hydrocarbons vs. total organic carbon. *AAPG Bull* 74: 799–804.
92. Allen PA, Allen JR (2013) *Basin Analysis: Principles and Application to Petroleum Play Assessment*, New York: Wiley-Blackwell.
93. Tissot BP, Welte DH (1984) *Petroleum Formation and Occurrence.* Springer-Verlag, New York.
94. Hartkopf-Fröder C, Königshof P, Littke R, et al. (2015) Optical thermal maturity parameters and organic geochemical alteration at low grade diagenesis to anchimetamorphism: A review. *Int J Coal Geol* 150–151: 74–119.
95. Barker CE, Pawlewicz MJ (1994) Calculation of vitrinite reflectance from thermal histories and peak temperatures. *Am Chem Soc* 570: 216–219.

96. Jarvie D (2018) Correlation of Tmax and measured vitrinite reflectance. Available from: https://www.wildcattechnologies.com/application/files/9915/1689/1979/Dan_Jarvie_Correlation_of_Tmax_and_measured_vitrinite_reflectance.pdf.
97. Héroux Y, Chagnon A, Bertrand R (1979) Compilation and correlation of major maturation indicators. *Am Assoc Pet Geol Bull* 63: 2128–2144.
98. Bird KJ, Burruss RC, Pawlewicz MJ (1999) Thermal maturity, Chapter VR. *U S Geol Surv Open File Rep* 98–34.
99. Kisch HJ (1991) Illite crystallinity: recommendations on sample preparation, X-ray diffraction settings, and interlaboratory samples. *J Metamorp Geol* 9: 665–670.
100. Merriman RJ, Peacor DR (1999) Very low-grade metapelites: mineralogy, microfabrics and measuring reaction progress. *Low-grade metamorphism*, Osney Mead, Oxford, 10–60.
101. Essene EJ (1989) The current status of thermometry in metamorphic rocks. *Geol Soc Am Spec Publ* 43: 1–44.
102. Frey M, de Capitani C, Liou JG (1991) A new petrogenetic grid for low-grade metabasites. *J Metamorp Geol* 9: 497–509.
103. Bousquet R, Oberhänsli R, Goffé B, et al. (2008) Metamorphism of metasediments at the scale of an orogen: a key to the Tertiary geodynamic evolution of the Alps. *Geol Soc London Spec Publ* 298: 393–411.
104. Liou JG (1971) Synthesis and stability relations of prehnite, $Ca_2Al_2Si3_3O_{10}(OH)_2$. *Am Mineral* 56: 507–531.
105. Boles JR, Coombs DS (1975) Mineral reactions in zeolite Triassic tuff, Hokonui Hills, New Zealand. *Geol Soc Am Bull* 86: 163–173.
106. Wantanabe N, Numakura T, Sakaguchi K, et al. (2017) Potentially exploitable supercritical geothermal resources in the ductile crust. *Nat Geosci* 10: 140–144.
107. Liou JG (1970) Synthesis and stability relations of wairakite, $CaAl_2Si_4O_{12}{\cdot}2H_2O$. *Contrib Mineral Petrol* 27: 259–282.
108. Thompson AB (1970) Laumontite equilibria and the zeolite facies. *Am J Sci* 269: 267–275.
109. Schmidt D, Schmidt STh, Mullis J, et al. (1997) Very low-grade metamorphism of the Taveyanne formation of western Switzerland. *Contrib Mineral Petrol* 129: 385–403.
110. McSween HY, Labotka TC, Viviano-Beck CE (2015) Metamorphism in the Martian crust. *Meteorit Planet Sci* 50: 590–603.
111. Weaver CE (1989) Clays, Muds and Shales. *Developments in Sedimentology 44*, Elsevier: Amsterdam.
112. Aldega L, Corrado S, Grasso M, Maniscalco R (2007) Correlation of diagenetic data from organic and inorganic studies in the Appeninic-Maghrebian fold-and-thrust belt: A case study from eastern Sicily. *J Geol* 115: 335–353.
113. Frey M (1987) *Very low-grade metamorphism of clastic sedimentary rocks.* Bishopbriggs, Glasgow, 9–58.
114. Burkhard M (1993) Calcite twins, their geometry, appearance and significance as stress-strain markers and indicators of tectonic regime: a review. *J Struct Geol* 15: 351–368.
115. Mullis J, Mählmann RF, Wolf M (2017) Fluid inclusion microthermometry to calibrate vitrinite reflectance (between 50 and 270°C), illiteKübler-index data and the diagenesis/anchizone boundary in the external part of the Central Alps. *Applied Clay Science* 143: 307–319.

116. Bernet M, Garver JI (2005) Fission-track analysis of detrital zircon. *Rev Mineral Geochem* 58: 205–237.
117. Sweeney JJ, Burnham AK (1990) Evaluation of a simple model of vitrinite reflectance based on chemical kinetics. *Am Assoc Pet Geol Bull* 74: 1559–1570.
118. McMillan R, Golding M 92019) Thermal maturity of carbonaceous material in conodonts and the Color Alteration Index: independently identifying maximum temperature with Raman spectroscopy. *Palaeogeogr Palaeoclimatol Palaeoecol* 534: 1–11.
119. Coombs DS (1961) Some recent work on the lower grades of metamorphism. *Aust J Sci* 24: 203–215.
120. Sclater JG, Christie PAF (1980) Continental Stretching: An Explanation of the Post-Mid-Cretaceous Subsidence of the Central North Sea Basin. *J Geophys Res* 85: 3711–3739.
121. Angevine CL, Heller PL, Paola C (1990) Quantitative sedimentary basin modeling. *Am Assoc Pet Geol*.
122. Ernst WG (1996) Petrochemical study of regional/contact metamorphism in metaclastic strata of the central White-Inyo Range, eastern California. *Geol Soc Am Bull* 108: 1528–1548.
123. Wang W, Clarke G, Daczko NR, et al, (2018) Modelling the partial melting of metasediments in a low-pressure regional contact aureole: the effect of water and whole-rock composition. *Geol Mag* 156.
124. Kays MA (1970) Mesozoic metamorphism, May Creek Schist Belt, Klamath Mountains, Oregon. *Geol Soc Am Bull* 81: 2743–2758.
125. Barton MD, Battles DA, Debout GE, et al. (1988) Mesozoic contact metamorphism in the western United States. *Metamorphism and crustal evolution of the western United States*, Prentice Hall, 110–178.
126. Shaw CA, Snee LW, Selverstone J, et al. (1999) 40Ar/39Ar Thermochronology of Mesoproterozoic Metamorphism in the Colorado Front Range *J Geol* 107: 49–67.
127. Ratschbacher L, Franz L, Enkelmann E, et al. (2006) The Sino-Korean-Yangtze suture, the Huwan detachment, and the Paleozoic-Tertiary exhumation of (ultra) high-pressure rocks along the Tongbai-Xinxian- Dabie Mountains. *Geol Soc Am Spec Pap* 403: 45–75.
128. Berman RG, Ryan JJ, Gordey SP, et al. (2007) Permian to Cretaceous polymetamorphic evolution of the Stewart River region, Yukon-Tanana terrane, Yukon, Canada: P-T evolution linked with in situ SHRIMP monazite geochronology. *J Metamorp Geol* 25: 803–827.
129. Wintsch RP, Yang HJ, Li XH, et al. (2011) Geochronologic evidence for a cold arc–continent collision: The Taiwan orogeny. *Lithos* 125: 236–248.
130. Hamilton BM, Pattison DR, Sanborne-Barrie M, et al. (2012) Preliminary characterization of metamorphism on Cumberland Peninsula, Baffin Island, Nunavut. *Geol Surv Can Curr Res*.
131. Viete DR, Oliver GJH, Fraser GL, et al. (2013) Timing and heat sources for the Barrovian metamorphism, Scotland. *Lithos* 177: 148–163.
132. McClelland WC, Mattinson JM (2000) Cretaceous-Tertiary evolution of the western Coast Mountains, central southeastern Alaska. *Geol Soc Am Spec Pap* 343: 159–182.
133. Stowell RR, Crawford ML (2000) Metamorphic history of the Coast Mountains orogen, western British Columbia and southeastern Alaska. *Geol Soc Am Spec Pap* 343: 257–283.
134. Trop JM, Benowitz JA, Koepp DO, et al. (2020) Stitch in the ditch: Nutzotin Mountains (Alaska) fluvial strata and a dike record ca. 117-114 Ma accretion of Wrangellia with western North America and initiation of the Totschunda fault. *Geosphere* 16: 82–110.

135. Shepard GE, Mülle r RD, Seton M (2013) The tectonic evolution of the Arctic since Pangea breakup: Integrating constraints from surface geology and geophysics with mantle structure. *Earth-Sci Rev* 124: 148–183.
136. Sigloch K, Mihalynuk MG (2017) Mantle and geological evidence for a Late Jurassic-Cretaceous suture spanning North America. *Geol Soc Am Bull* 129: 1489–1520.